Review paper

Cite as: Adler RS: Musculoskeletal ultrasound: a technical and historical perspective. J Ultrason 2023; 23: e172–e187. doi: 10.15557/JoU.2023.0027.

Submitted: 08.07.2023
Accepted: 21.08.2023
Published: 30.10.2023

Musculoskeletal ultrasound: a technical and historical perspective

Ronald Steven Adler

Department of Radiology, New York University, Grossman School of Medicine, Langone Orthopedic Center, New York, USA

Correspondence: Ronald Steven Adler; e-mail: ronald.adler@nyulangone.org

DOI: 10.15557/JoU.2023.0027

Keywords
ultrasound; musculoskeletal; technical; historical

Abstract

During the past four decades, musculoskeletal ultrasound has become popular as an imaging modality due to its low cost, accessibility, and lack of ionizing radiation. The development of ultrasound technology was possible in large part due to concomitant advances in both solid-state electronics and signal processing. The invention of the transistor and digital computer in the late 1940s was integral in its development. Moore's prediction that the number of microprocessors on a chip would grow exponentially, resulting in progressive miniaturization in chip design and therefore increased computational power, added to these capabilities. The development of musculoskeletal ultrasound has paralleled technical advances in diagnostic ultrasound. The appearance of a large variety of transducer capabilities and rapid image processing along with the ability to assess vascularity and tissue properties has expanded and continues to expand the role of musculoskeletal ultrasound. It should also be noted that these developments have in large part been due to a number of individuals who had the insight to see the potential applications of this developing technology to a host of relevant clinical musculoskeletal problems. Exquisite high-resolution images of both deep and small superficial musculoskeletal anatomy, assessment of vascularity on a capillary level and tissue mechanical properties can be obtained. Ultrasound has also been recognized as the method of choice to perform a large variety of interventional procedures. A brief review of these technical developments, the timeline over which these improvements occurred, and the impact on musculoskeletal ultrasound is presented below.

Introduction

During the past four decades, Musculoskeletal Ultrasound (MSKUS) has become popular as an imaging modality, particularly outside the United States, due to its low cost, accessibility, and lack of ionizing radiation. The development of MSKUS has paralleled technical advances in diagnostic ultrasound, from the earliest images displaying bistable images of musculoskeletal anatomy to its current state, where exquisite images of muscles, tendons, nerves, ligaments and joints can be obtained[1–6]. With ongoing technical improvements in the quality of grayscale imaging along with some newer applications, such as shear wave elastography, enabling functional assessment of the musculoskeletal soft tissues, MSKUS is becoming ubiquitous[7–10].

The compactness of some of the currently available scanners makes this modality conducive to bedside imaging as well as imaging in remote settings[11–13] (Fig. 1). One of the most popular applications of MSKUS has been to provide guidance for a large variety of interventional procedures, since it allows visualization of the relevant anatomy and needle position in real time[14] (Fig. 2, Fig. 3). In addition to radiology, the modality has opened itself up to wider usage by a large variety of clinical subspecialties involved in treating patients with musculoskeletal diseases, as well as anesthesiologists/pain management physicians who perform nerve blocks, therapeutic or ablative procedures of peripheral nerve lesions[4–8,10].

Technical advances

Ultrasound technology has undergone extraordinary growth since its inception in the 1940s[15–18]. A brief description of technological developments in ultrasound allows a greater perspective as to the timing when various MSKUS applications first appear. The development of ultrasound technology was possible in large part due to concomitant advances in both solid-state electronics and signal processing. The invention of the transistor and digital computer in the late 1940s was integral in the development of ultrasound technology[18,19]. Gordon Moore in 1964 predicted that the number of microprocessors on a chip would grow exponentially over time. This growth would result in progressive miniaturization of chip design and, therefore, increased computational power.

One of the earliest presentations of ultrasound data employed pulse echo techniques, derived from earlier radar applications. This in-

Fig. 1. A. *Compact ultrasound system with wireless chargeable transducers. A 10 MHz linear transducer is displayed. Some of the functionality normally reserved for the scanner has been incorporated into the transducer architecture, including beam forming, steering, and some image processing.* **B.** *An early laptop system utilized in a remote setting (Ghana, 2004) for guidance for therapeutic injection*[11]

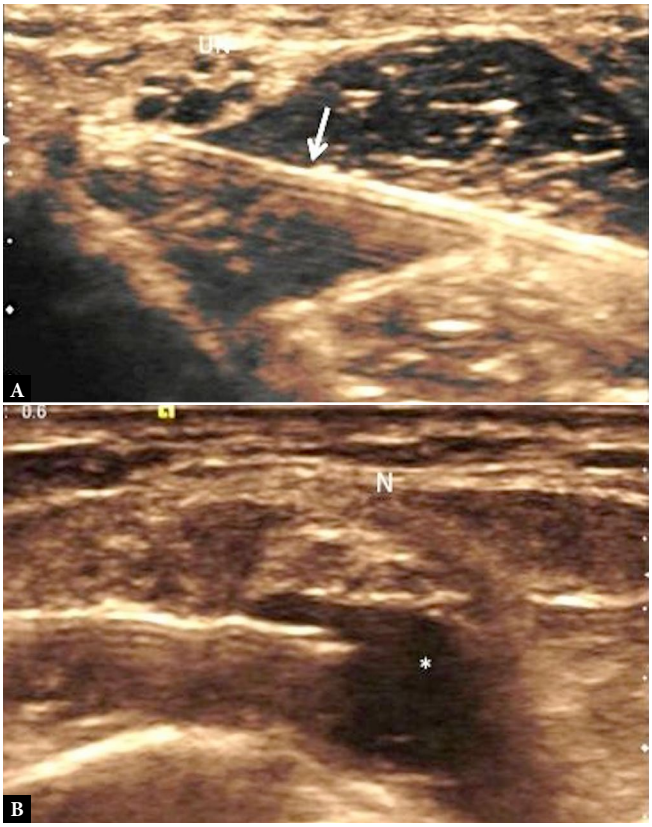

Fig. 2. *Guided interventions with precise needle localization.* **A.** *A 25-gauge hypodermic needle (arrow) is shown adjacent to the outer epineurium of the ulnar nerve (un) for purposes of hydrodissection and perineural steroid injection.* **B.** *Anesthetic (*) surrounds the medial plantar nerve (N) during performance of a nerve block. The 25-gauge hypodermic needle is well delineated on ultrasound and monitored in a real-time mode as well as the distribution of the injectate*

volved the display of individual A-line data, assuming a fixed speed of sound in soft tissue[15]. Each A-line represented the intensity of acoustic backscatter at various depths, adjusted for attenuation. Placing this in a time-varying display allows the display of M-mode data, typically utilized in cardiology[15].

Musculoskeletal soft tissues typically present strong reflecting surfaces (specular reflectors) along with complex internal morphology. A unique feature of many of these tissues is an internal fibrillar architecture, most prominent in tendons[20], as well as a linear orientation. One of the most useful features of MSKUS is its real-time nature, allowing the performance of provocative maneuvers and providing real-time guidance during an intervention[21–23]. The ability to visualize features that are useful for musculoskeletal imaging entails two requirements: the display of the back-scattered data as a 2-D anatomic image and rapid acquisition/display (15–20 frames per second) of the image data. The first real-time 2-D scanners were introduced in the late 1960s, involving one or two crystals undergoing translation or rotation to produce a composite bistable image[15–17,24] (Fig. 4).

Ultrasound did not become a widely accepted diagnostic tool, though, until the early 1970s, when grayscale ultrasound, in which non-linear echo amplitudes are mapped to gray levels, became the method of choice to display image data[15–17]. The development of multi-element linear phased array transducers, employing digital image processing, allowed the display of 2-D grayscale images. Duplex ultrasound scanners began to appear during this period, allowing the imaging of anatomy and the measurement of blood flow in a single scanner[18]. These systems appeared in the late 1970s/early 1980s. Some of the earliest images of extremity anatomy, hematomas in muscle, large joint effusions/synovitis appeared as extended-field-of-view (EFOV) B-mode images[25–32]. In 1985, the first color Doppler flow-mapping system that combined Doppler flow imaging in color with B-mode imaging in grayscale was introduced[15–17].

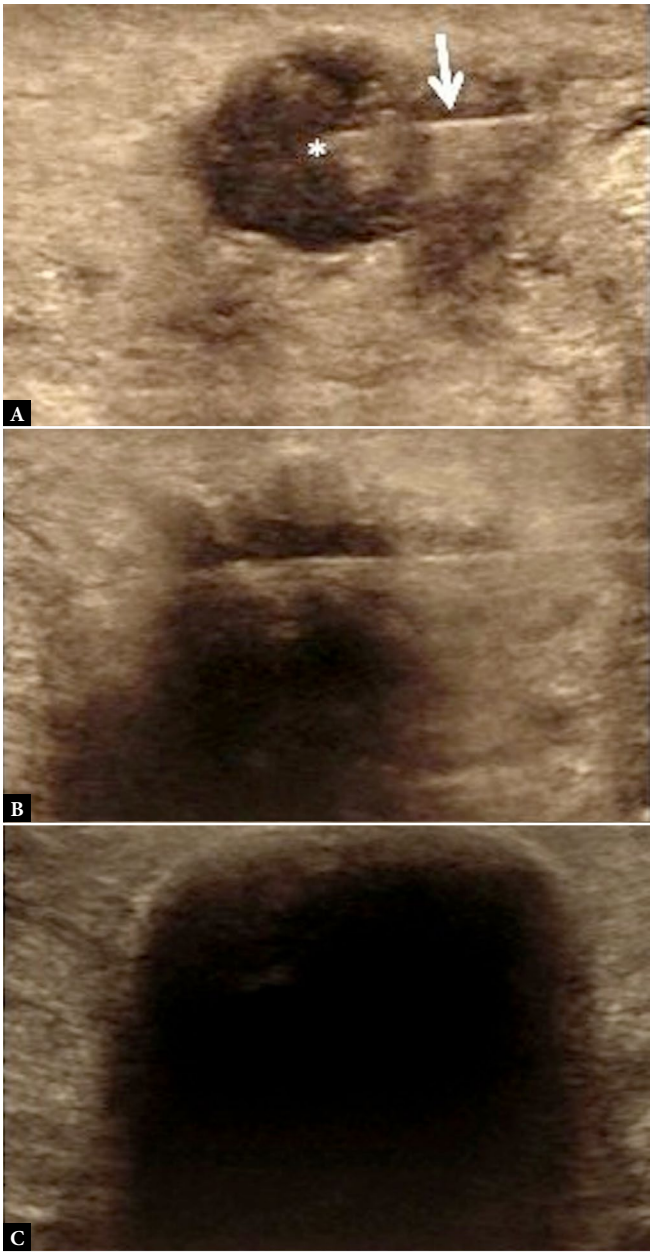

Fig. 3. *Ablative procedure.* **A.** *A hypoechoic nodule (*)in a patient with a symptomatic second web space interdigital neuroma. A portion of a 17 gauge cryoablation probe (arrow) is evident passing through the center of the neuroma.* **B** *and* **C.** *Progressive development of an ice ball observed in real time, for purposes of ablation of the plantar digital nerve encompassed by the neuroma. Dense posterior acoustic shadowing followed by a curvilinear specular reflector (superficial margin of the ice ball) is apparent. Ultrasound guidance allows precise targeting of the lesion*

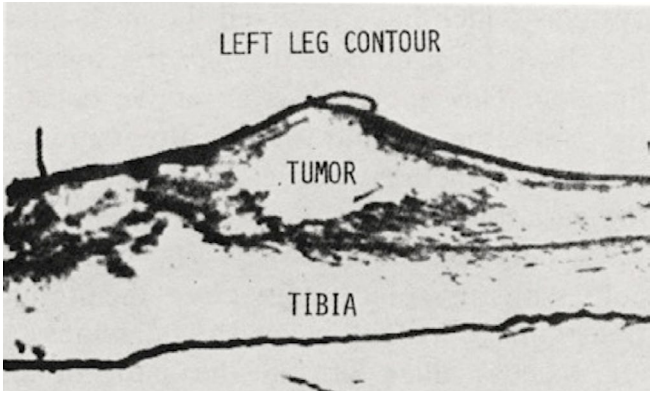

Fig. 4. *Bistable image of calf rhabdomyosarcoma (1976) produced with a translating 2.5 MHz transducer[24]. Printed with permission of Dr. Paul Carson. The tumor is labeled as is the tibial cortex (tibia)*

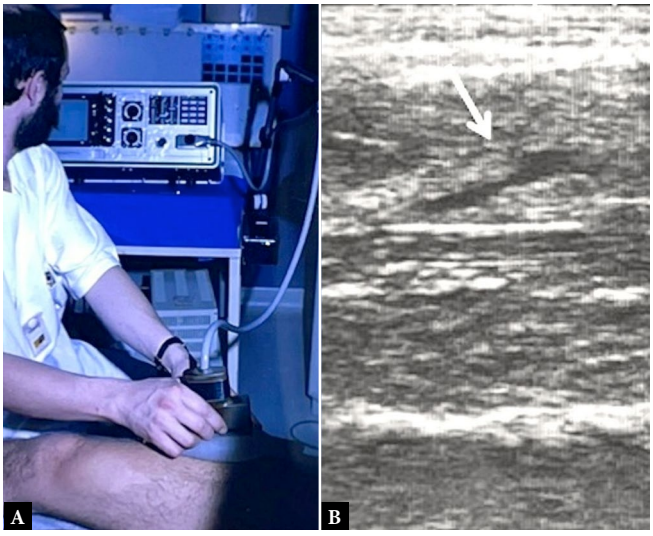

Fig. 5. A. *Early B-mode ultrasound scanner with first commercially available 5 MHz linear phased array transducer. Scans of the quadriceps muscles in a soccer player (1979–1980).* **B.** *Static image (1983) shows an obliquely oriented tear in the rectus femoris (arrow). Printed with permission of Dr. Bruno Fornage*

By 1980, commercial real-time phased array imaging systems were made possible by developments in video microprocessors, digital memory, and the miniaturization offered by programmable integrated circuits. During the 1980s, multi-element array systems allowed rapid growth of transducer technology. Improved materials and piezoelectric composites enabled the production of arrays with several hundred elements, operating at higher frequencies and wider bandwidths. This enhanced flexibility allowed the imaging and operation of other modes within the same transducer at multiple frequencies selectable by the user[18].

With the appearance of these new systems in the 1980s, the applications to the MSK system started to appear at a greater frequency in the imaging literature. Examination of articular cartilage, joint effusions, synovitis, tendon and muscle abnormalities, and nerve imaging using grayscale ultrasound were described, including the first descriptions of tendon morphology and anisotropy[20–22,32–46]. Multiple anatomic locations were accessible to this modality, resulting in studies of the Achilles tendon, patellar tendon, and soon also more complex anatomical areas such as the rotator cuff[22,39–40] (Fig. 5, Fig. 6, Fig. 7). Early assessment of muscle hematomas and soft tissue masses using bistable techniques expanded to more sophisticated descriptions of muscle and other soft tissue pathology[26–30,33,36]. Large joints, such as the knee and hip, were ultimately expanded to include small joint pathology, such as in the hands and feet[41,45]. The real-time capabilities provide a method to assess static anatomy as

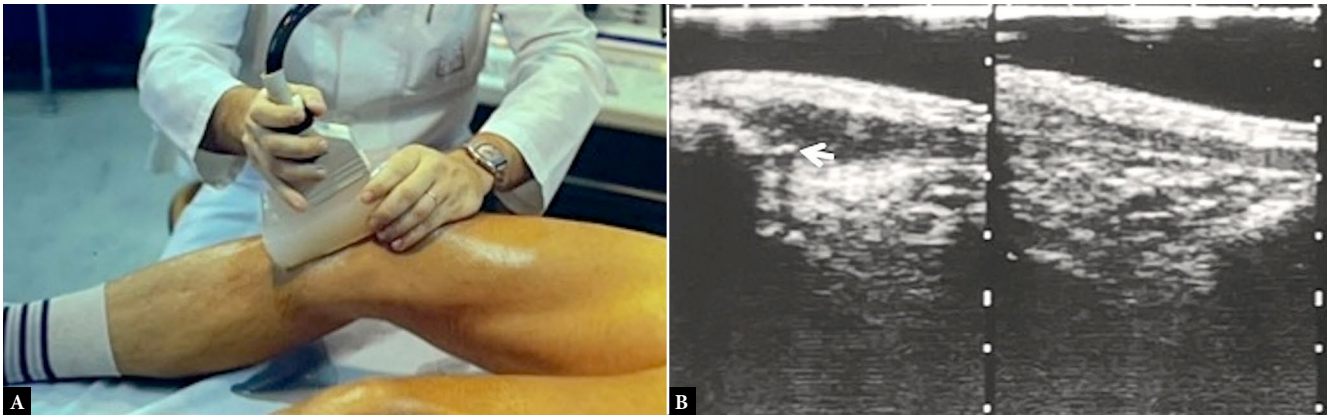

Fig. 6. A. *5 MHz scans of patellar tendons with knee in flexion (1982) using a homemade standoff pad to place the tendon into the focal zone of the transducer.* **B.** *Grayscale image of the left symptomatic side shows thickened hypoechoic tendon with proximal intra-tendinous calcification evident (arrow) and the right normal side for comparison. Printed with permission of Dr. Bruno Fornage*

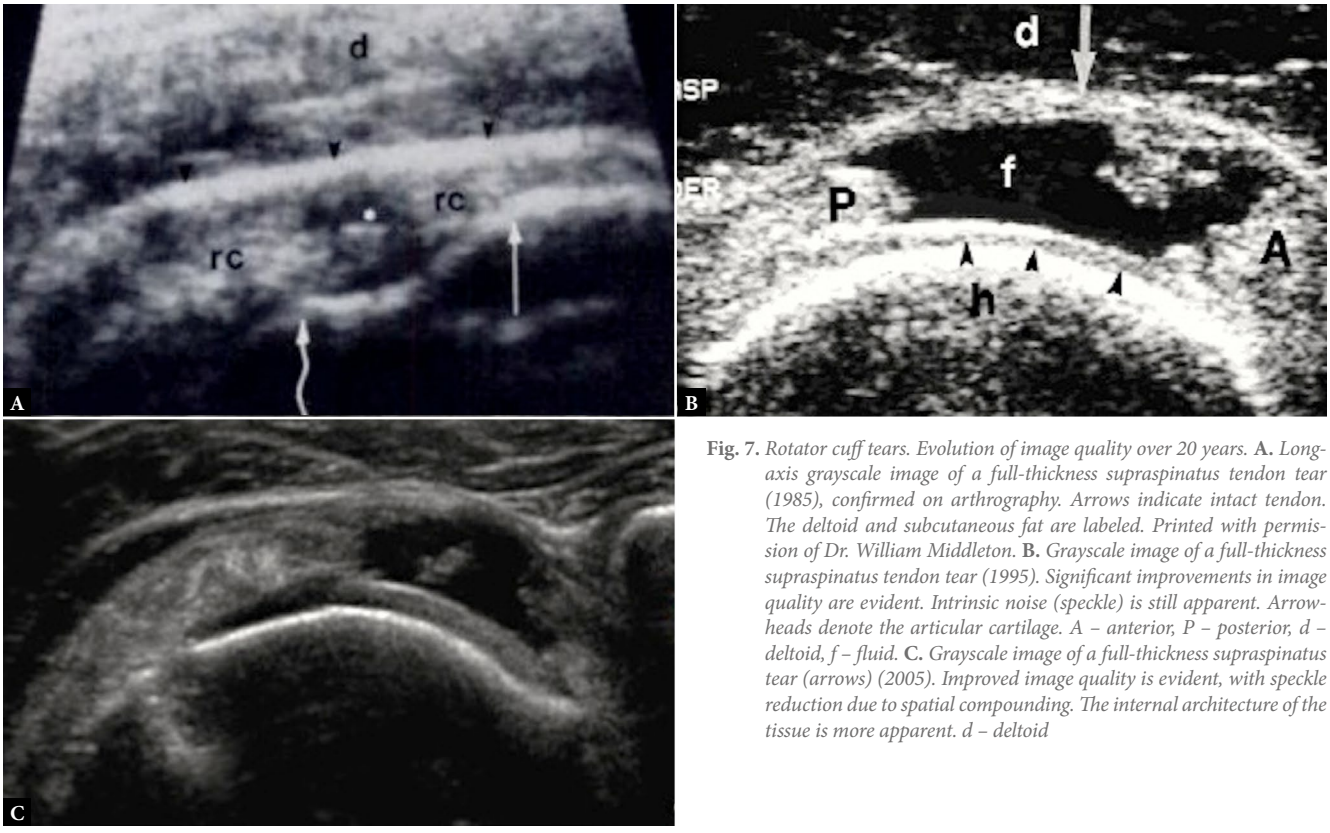

Fig. 7. *Rotator cuff tears. Evolution of image quality over 20 years.* **A.** *Long-axis grayscale image of a full-thickness supraspinatus tendon tear (1985), confirmed on arthrography. Arrows indicate intact tendon. The deltoid and subcutaneous fat are labeled. Printed with permission of Dr. William Middleton.* **B.** *Grayscale image of a full-thickness supraspinatus tendon tear (1995). Significant improvements in image quality are evident. Intrinsic noise (speckle) is still apparent. Arrowheads denote the articular cartilage. A – anterior, P – posterior, d – deltoid, f – fluid.* **C.** *Grayscale image of a full-thickness supraspinatus tear (arrows) (2005). Improved image quality is evident, with speckle reduction due to spatial compounding. The internal architecture of the tissue is more apparent. d – deltoid*

well as pathology that manifests when accentuated by some maneuver. Examples include neonatal hip examination, assessment of joint effusions as well as examination of rotator cuff impingement[38,42–43].

By the 1990s, developments enabling more rapid image acquisition and the availability of low cost analog to digital (A/D) chips improved computational capabilities, resulting in faster image processing in smaller devices that could be assembled at a lower cost[18]. Imaging systems incorporating these advances evolved into digital architectures and beam formers, permitting beam steering and electronic focusing. The most dramatic changes have been through the continual miniaturization of electronics in accordance with Moore's law[19]. Smaller size components led to the first commercially available phased array imaging systems as well as new portable imaging systems that weigh only a few pounds[13] (Fig. 1). The current generation of scanners include 1½ and 2-dimensional arrays allowing improved in- and out-of-plane (elevational) focusing, rapid image processing, and 3-D and 4-D imaging (real-time volumetric imaging)[47–52] (Fig. 7, Fig. 8).

Specific technical developments

The potential utility of ultrasound in evaluating the musculoskeletal system evolved to its current state through a series of advances spanning the 1980s through the first decade of the 21st century. Many

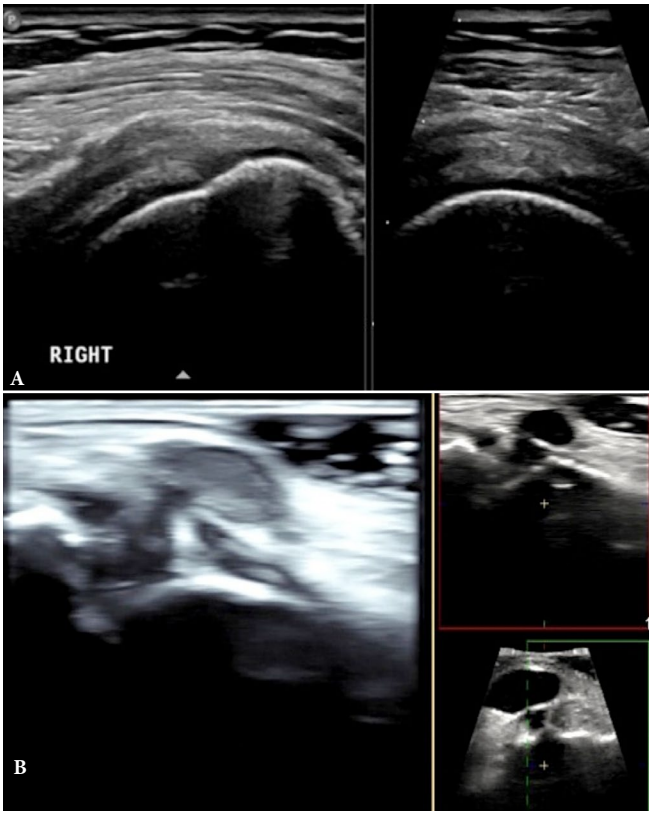

Fig. 8. A. *Biplanar real-time grayscale image of the rotator cuff derived from a 14 MHz matrix array transducer.* **B.** *3D acquisition of a dorsal ganglion cyst using a 14 MHz matrix array transducer shows simultaneous images of the cyst in two orthogonal planes as well as volume rendering of the cyst*

of these features are incorporated in present-day clinical scanners, including assessment of soft tissue vascularity, improvements in anatomic depiction of the relevant musculoskeletal anatomy, and enhanced characterization of soft tissue composition.

Blood flow

Assessment of vascularity plays an important role in musculoskeletal imaging. Inflammation, repair processes, and a variety of musculoskeletal tumors display diverse degrees of vascularity which can serve as a measure of disease activity and/or response to a therapeutic intervention.

Doppler techniques date back to the 1950s, and began to play an important clinical role once incorporated as part of a duplex imaging package within the ultrasound scanner[16]. Vascular assessment was further enhanced with the introduction of color Doppler in the 1980s, in which the mean frequency Doppler shift within an interrogated pixel could be color-encoded to reflect mean velocity and direction, producing an anatomic map of vascularity. A series of adjustable parameters and internal discriminators were available to help differentiate true flow from artifact due to low-frequency soft tissue motion. Color Doppler continues to be an important tool in depicting high flow states.

In the musculoskeletal system, vascularity is characteristically low flow and often poly-directional. The limitations associated with color Doppler maps include aliasing and drop out of signal when insonating at 90 degrees, as per the Doppler equation. Increasing color gain to improve flow sensitivity has the effect of introducing low-amplitude noise in the color-encoded image. Many of these issues were resolved with the recognition that flow sensitivity could be improved by encoding the demodulated Doppler signal intensity in color, with the assumption that the noise floor is of low amplitude[53] (Fig. 9).

Power Doppler (PD), as it has become known, described in the mid-1990s, significantly improved sensitivity to low-flow states, making it ideal for musculoskeletal imaging[54–58]. PD is not subject to aliasing artifact and it is not as sensitive to the insonation angle. PD was established to be a good indicator of hyperemic inflammatory states, capable of depicting blood flow in soft tissues more readily than conventional color Doppler (Fig. 10). PD has, in fact, become an important tool in assessing disease activity in inflam-

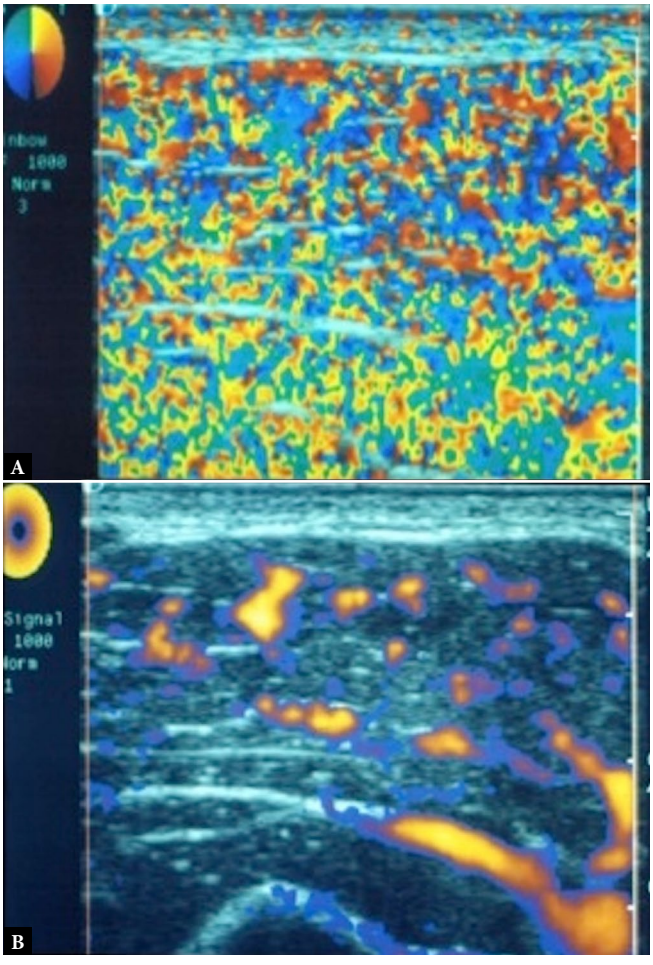

Fig. 9. *Power Doppler (***B***) and color Doppler (***A***) ultrasound images of the biceps muscle seen in cross-section, using the same color gain settings and transducer. The color gain has been increased, resulting in color noise completely filling the color Doppler image. Even though the noise is of low power, it encompasses all possible frequency shifts. In the power Doppler (PD) image, an amplitude filter has been applied, excluding low power contributions below a fixed threshold. As a result, only the vessels are displayed, superimposed on the normal grayscale appearance of the biceps muscle*

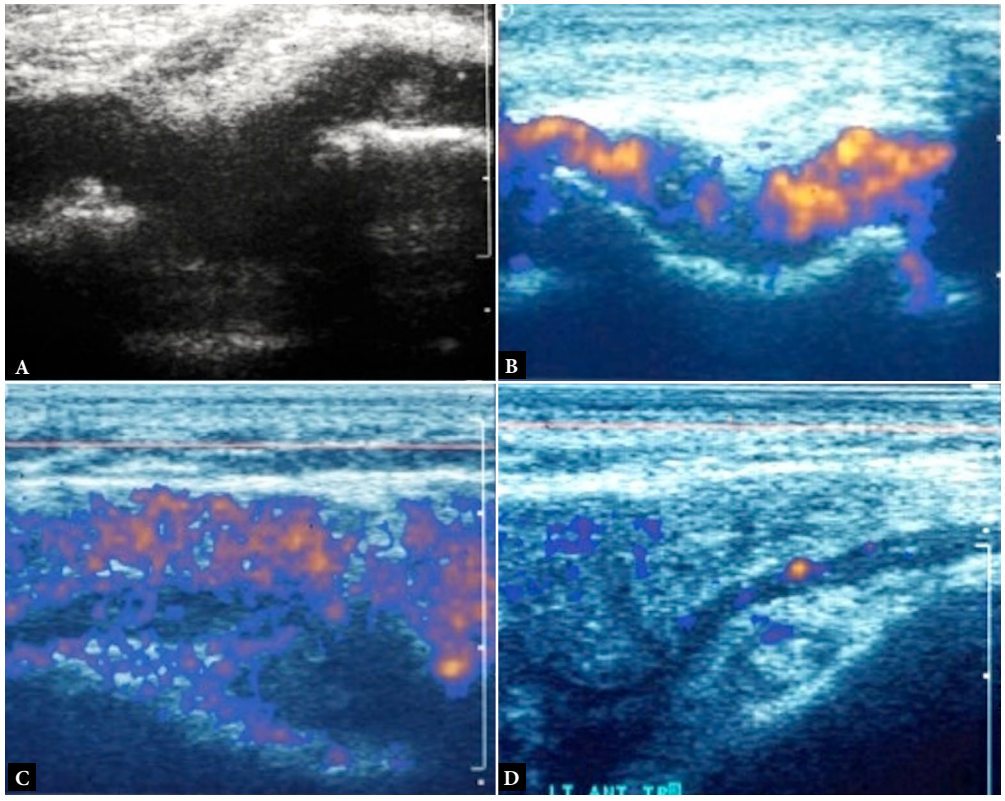

Fig. 10. *Synovial hyperemia on power Doppler (PD) ultrasound using the first commercially available system with PD capability in the elbow of a patient with rheumatoid arthritis (1994).* **A**. *Extensive hypoechoic soft tissue (arrows) representing inflammatory pannus is evident.* **B.** *On PD, marked hyperemia present in the hypoechoic soft tissue is compatible with active synovitis.* **C.** *One of the first demonstrations of response to therapy using power Doppler ultrasound (1995) in a patient with septic bursitis at initial presentation.* **D.** *Two weeks after surgical incision and drainage and placement on antibiotics. The same Doppler parameters were used in both images. There was a marked decrease in the extent of hyperemia, even though the grayscale appearance continued to be abnormal*

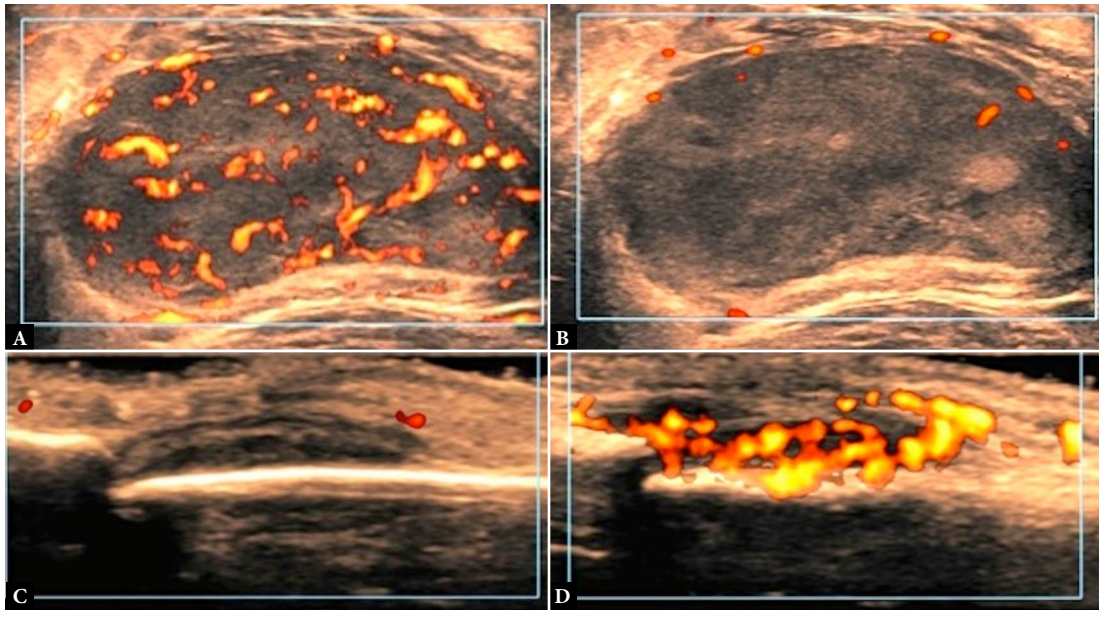

Fig. 11. *Power Doppler (PD) ultrasound image (***B***) and microvascular flow (Slow Flow ™) image (***A***) of a soft tissue sarcoma within the rectus femoris muscle using identical Doppler parameters. Significant improvement in sensitivity and vascular morphology without blooming artifact is evident in the microvascular flow image. The mass appears hypovascular on PD, whereas the Slow Flow image depicts a hypervascular mass.* **C.** *Patient with swollen left 3rd PIP joint and history of psoriasis. PD (left) and Slow Flow image (right) long-axis views of the dorsal recess. There is mild distension of the dorsal capsule by hypoechoic soft tissue. Minimal periarticular vascularity is depicted on PD.* **D.** *On Slow Flow, there is marked synovial and periarticular hyperemia*

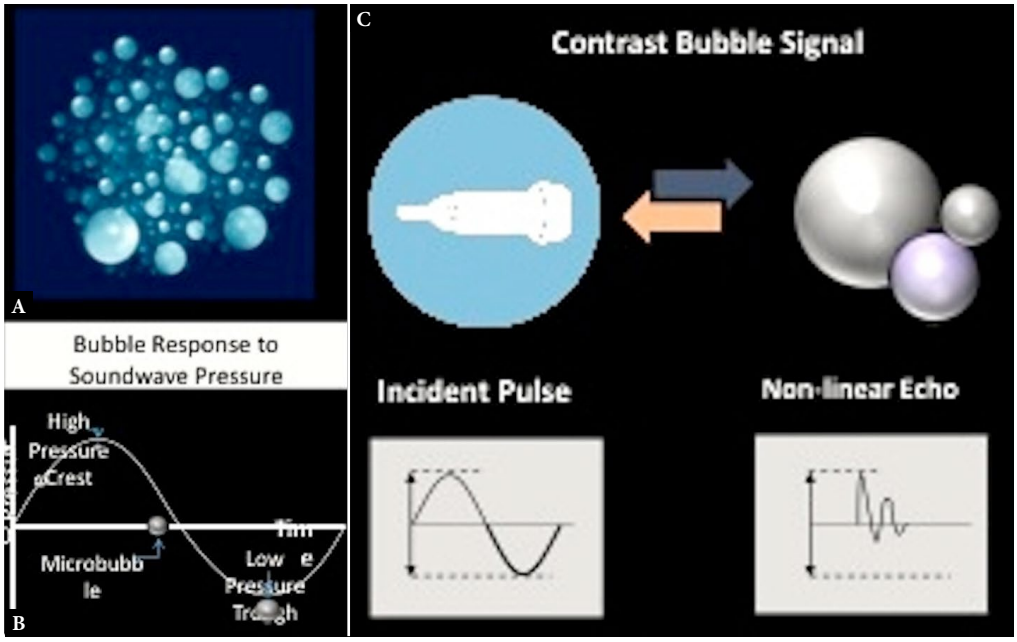

Fig. 12. *Contrast agents.* **A.** *Microbubbles made up of a gas core with a flexible, biocompatible containment shell which is usually phospholipid but can also be a protein, such as albumin. Bubble size typically varies between 2–10 microns.* **B.** *The insonating beam operates at the resonant frequency, which is dependent on bubble size. Microbubbles in the ultrasound field react to pressure by changing size, based on the pressure amplitude of the insonating beam as indicated.* **C.** *The resultant scattered echoes are non-linear, which can be represented as an expansion consisting of the fundamental along with higher harmonic components. The goal of contrast imaging is to remove the fundamental component (e.g. tissue contribution) and image the second harmonic. Images printed with permission of Siemens medical systems*

matory arthritis[58]. An added bonus is that PD is more amenable to semi-quantitative estimates of vascularity, noting that it can provide a measure of fractional moving blood volume[59]. A fundamental problem with PD, however, is the presence of so-called blooming artifact, due to high-amplitude low-frequency motion at tissue interfaces (clutter)[60].

In the current generation of high-end ultrasound scanners, blooming artifact is significantly improved by employing newer clutter cancelling techniques, which are computationally intensive, requiring high-frame rates and long ensemble lengths[60–62]. These adaptive filters have a number of different names (slow flow, microvascular flow, etc.), but they generally involve separation of the weakly scattering blood flow from low-frequency motion of strong reflecting tissue boundaries. These microvascular flow techniques are stillbeing investigated, but they appear to improve flow sensitivity and depiction of vascular anatomy, while eliminating blooming artifact[61–62] (Fig. 11).

Ultrasound contrast agents

The most significant improvement in flow detection, however, occurs with the inclusion of ultrasound contrast agents, which are true capillary imaging agents. Contrast agents have long been investigated in ultrasound, dating back to 1968, with the observation that microbubbles produce strong reflections on ultrasound[63]. This led to intensive research in micro-bubble contrast agents extending into the 1970s–80s, with the first clinically available agent released in 1984. The current (second) generation of contrast agents exhibit a good safety profile and have been used extensively in cardiology and abdominal imaging applications[64].

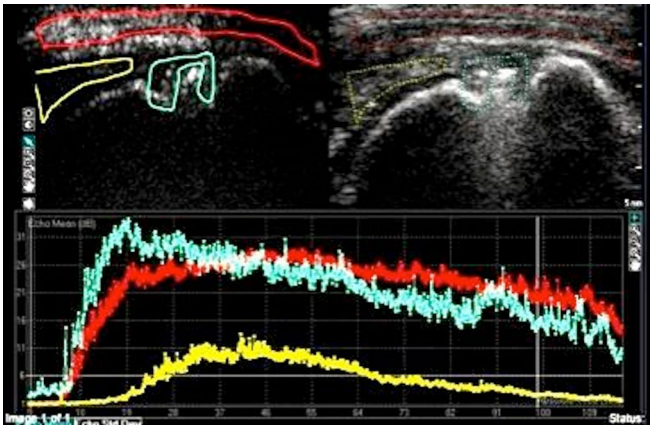

Fig. 13. *Time-intensity curve. Composite image obtained from a contrast study of a patient three months out from rotator cuff repair. The upper right image shows a long-axis image of the supraspinatus tendon repair with a single suture anchor evident. The upper left image displays a single frame from a contrast study with three ROIs around the suture anchor site, proximal tendon and peribursal soft tissues. A time-intensity curve (bottom) is depicted for each ROI, using the same color scheme as the ROI boundaries*

Present-day contrast agents are encapsulated microbubbles (1–10 microns in size) that undergo strong backscatter at certain resonant frequencies and are readily detectable, using harmonic imaging (discussed below)[65] (Fig. 12). These agents are injected intravenously, pass through the pulmonary capillary bed, and then appear in the arterial phase. The bubbles have a half-life of several minutes and the gas is ultimately exhaled in the lungs, while the outer shell is metabolized[64].

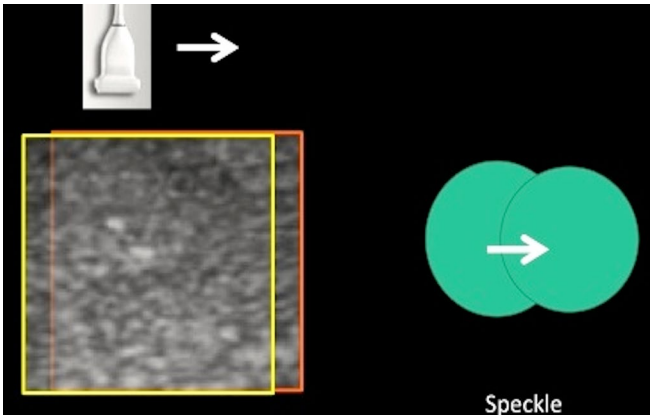

Fig. 14. *Speckle distribution in 2D image consists of sub-resolution scatterers that are randomly distributed in space. A small lateral translation by the transducer (arrow, left image) results in a new speckle field. Provided the translation is sufficiently small (within a correlation length), the speckle can be used to estimate the degree and angle of translation (right image), allowing for image registration. Alternatively, if the displacements are too large, the images are uncorrelated. In the case of spatial compounding, where a rotation is involved, the angular displacements are sufficiently large for the speckle to decorrelate, and only the specular reflectors contribute to the final image*

Contrast agents have been used in the imaging of the musculoskeletal system in a limited fashion over the last two decades. They have been shown to allow robust quantification of vascularity and blood flow, but fall into the category of off-label usage in the United States. Contrast has allowed remarkably improved flow sensitivity in the detection and quantification of hyperemic states, such as inflammatory myopathies, inflammatory arthritis, tendinosis and tendon repairs[66–72] (Fig. 13, Video 1). In addition to improved flow sensitivity and flow quantification, contrast agents may serve as therapeutic delivery agents in the future[64].

Speckle

The advent of grayscale imaging has allowed the assessment of internal tissue morphology[16]. A feature of grayscale images is the appearance of an inherent granular noise within the image, known as speckle[73] (Fig. 14). The latter arises due to small inhomogeneities (e.g. variation in acoustic impedance) within the soft tissues that scatter ultrasound but are in and of themselves too small to resolve. Within a resolution element, there can be many such scatterers, which can only be characterized in a statistical sense[74,75]. Since these scatterers are fixed in space, small translations, rotations or compressions by the ultrasound transducers may contain some degree of correlation to the previous transducer position[76] (Fig. 14).

One method to achieve improved image quality, therefore, is to reduce the degree of unwanted speckle within the image. There are a variety of ways to accomplish this, one being temporal averaging (i.e. changing persistence), which has the effect of smoothing the image, while reducing spatial resolution and decreasing the frame rate[77–81]. One of the most successful methods to reduce speckle, which has significantly impacted musculoskeletal imaging, is spatial compounding using speckle decorrelation[81–82] (Fig. 15). In this latter technique, image data from multiple look directions (as many as eight) are averaged, producing a speckle-free image with improved signal-to-noise ratio and an anatomically improved image. The one caveat in using spatial compounding is that certain artifacts which are sometimes diagnostically useful, such as posterior acoustic enhancement or refraction artifact, are diminished.

Speckle has played an important role in a number of applications that have impacted MSKUS. These applications utilize the fact that images derived from small changes in transducer positioning may remain correlated. Using this correlated motion gave rise to speckle tracking algorithms (late 1980s–early 1990s), which in turn provided an accurate method to produce in-plane image registration[76,83]. Examples include improved depiction of muscle and tendon pathology, selected soft tissue neoplasms and, in some cases, neural pathology.

Extended field-of-view (EFOV) imaging entails in-plane speckle tracking while manually translating the transducer to allow consecutive images to be combined into a single image depicting a larger anatomic region[84–86] (Fig. 16). This has led to improved depiction of pathology relative to adjacent anatomy as part of a large field-of-view image (up to approximately 60 cm). The advantage of EFOV imaging resides more in visualizing and describing an abnormal finding to clinicians or other imagers not present during the initial real-time assessment. Examples include depicting muscle and tendon tears, which are shown in relation to normal adjacent anatomy as well as al-

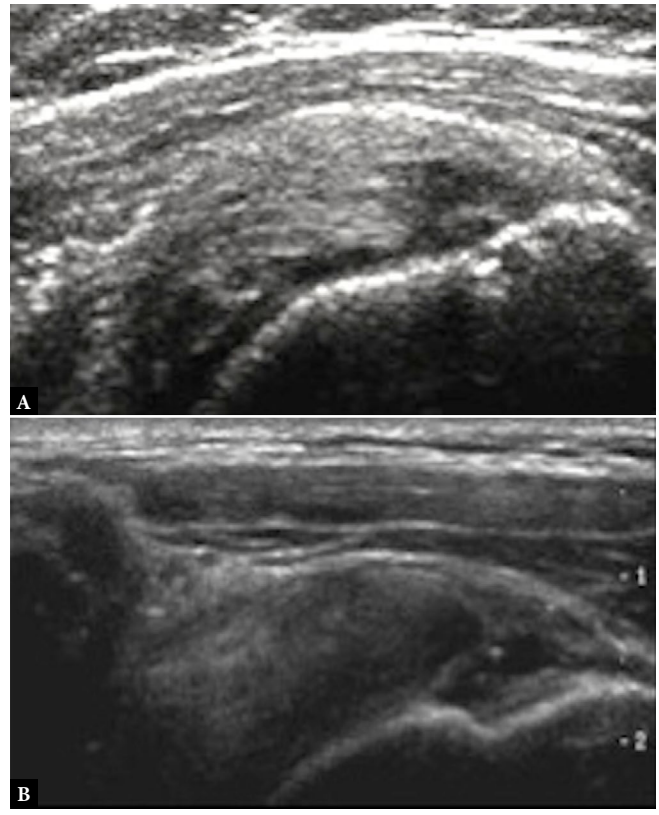

Fig. 15. *Spatial compounding. Both images display high-grade partial-thickness rotator cuff tears which are similar in morphology. The image labeled* **B** *is obtained with spatial compounding, while the image labeled* **A** *does not employ any spatial compounding. While both images are diagnostic, anatomic planes and tissue morphology are more distinct in the spatially compounded image. Cortical surfaces, tissue planes, and boundaries of the tear itself are better defined*

lowing the full extent of an abnormality to be displayed (Fig. 16). Obtaining these images remains somewhat of an art, though, since the tissue of interest is tracked using a free-hand technique. Poor speckle tracking and complex anatomy are potential complicating factors.

Elastography

Ultrasound elastography was initially described as an extension of soft tissue palpation, albeit in situations where an abnormality might not be clinically evident. The wide dynamic range of soft tissue mechanical properties is conducive to this type of imaging[87]. Thus, while research regarding soft tissue mechanical properties has been around since the 1970s, it was not until the 1990s that "sonopalpation" or compression-based elastography became clinically available[88–90]. This is a free-hand technique, whereby small compressions of soft tissue by the transducer result in small axial displacements that can be tracked using speckle tracking techniques. A strain map is obtained that is depth-dependent. The contrast derived in such a map is largely determined by the relative hardness of different tissues at the same depth[90]. While the technique is well-suited to small low-contrast soft tissue masses, it is less suitable for global tissue properties. Nevertheless, it has been used successfully in a variety of musculoskeletal applications, particularly tendinosis[91–92] (Fig. 17). There is an art to achieving optimal imaging by knowing what part of the compression/relaxation cycle to obtain measurements from and how light a touch is required. Most scanners have built-in tools to optimize the level of compression used, optimally producing 1–2% strain. A color map is generally employed, in which red denotes softer objects (greater strain or more deformable), while blue hues denote low strain (stiffer objects). The addition of a reference of known Young's modulus has been shown to be helpful in calculating relative strain in a manner that is more robust and less operator-dependent[93].

Another variant of elasticity imaging refers to the production of a shear wave either through direct mechanical means (transient elastography) or using the transducer itself to produce a push pulse (acoustic radiation force impulse imaging or ARFI)[94–98]. Historically, Doppler techniques have also been employed to detect the induced shear waves in transient elastography[96]. In either case, the transducer also serves to track the resultant shear wave propagation using a series of tracker pulses and speckle tracking to determine axial displacement at each element location (Fig. 18). The speed of the shear wave (measured in meters per second) reflects the local shear elastic (or equivalently Young's) modulus with the

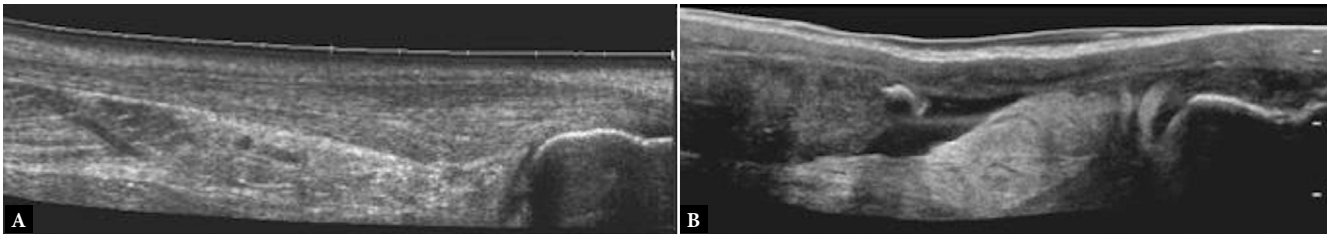

Fig. 16. *Extended field-of-view (EFOV) images of the Achilles tendon.* **A.** *The image is obtained from the first commercially available system that had EFOV capability. The full extent of the Achilles tendon is depicted, displaying mild enlargement proximal to its insertion on the calcaneus.* **B.** *The image of a torn Achilles tendon is obtained on a later generation scanner with speckle reduction. Again, the full extent of the tear and retracted fractured enthesophyte are readily depicted. The latter displays posterior acoustic shadowing. EFOV imaging allows an overall improved gestalt view of the pathology relative to conventional small field-of-view images*

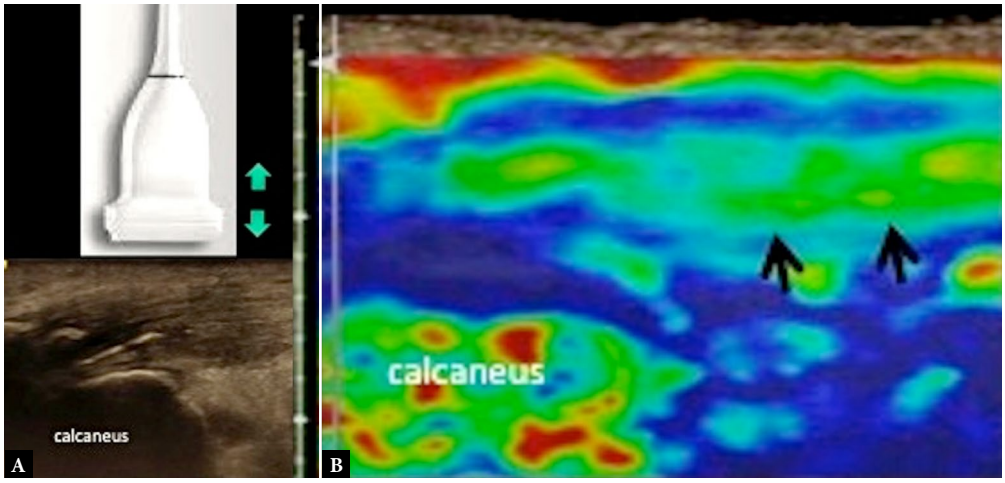

Fig. 17. *Patient with retrocalcaneal pain. Long-axis grayscale image of the Achilles tendon insertion (left) shows prominent enthesopathic mineralization. The deep surface of the tendon appears slightly hypoechoic relative to the superficial fibers, suggesting tendinosis. A rendition of the transducer is positioned over the distal tendon and low-amplitude compression/relaxation cycles are simulated to obtain an elastogram[92]. Compression elastogram (right) with image obtained during the mid-relaxation phase. The strain map is green in the deep fibers of the tendon (black arrows), corresponding to the hypoechoic region seen on the conventional grayscale image. There is improved contrast on the elastogram, and the degree of tendon softening appears more extensive in comparison. The standard color map is used, wherein higher strains (softer) are denoted in red hues, and low strain (stiff) in blue and green hues*

assumption that soft tissues are incompressible. While transient elastography may more accurately reflect the elastic moduli, ARFI techniques have been implemented in most high-end clinical scanners. The shear waves produced are generally bandwidth limited between approximately 100–1000 Hz, and the group velocity of the induced wave packet is estimated, which is then used to determine the Young's modulus[90].

Shear wave elastography (SWE) has a range of advantages: it is easy to implement, less operator-dependent, and produces a quantitative

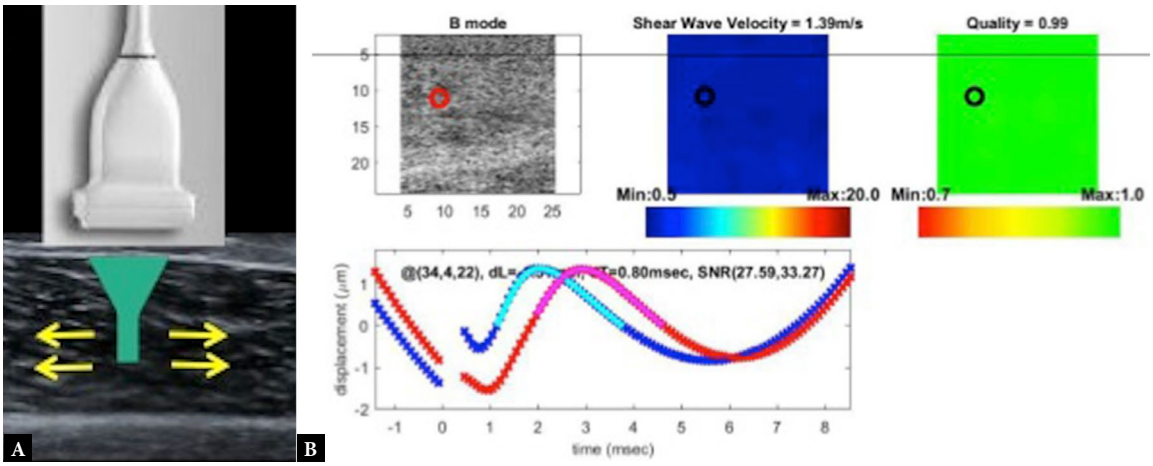

Fig. 18. A. *Representation of shear wave acquisition on normal skeletal muscle in long axis. A focused push pulse (acoustic radiation force impulse or ARFI) results in localized momentum transfer to the adjacent soft tissue. This in turn generates a cylindrically symmetric shear wave. Subsequently, the transducer elements are used to generate tracker pulses at a high frame rate.* **B.** *Generated shear wave produced through speckle tracking at two different transducer elements (point quantification) separated by approximately 2 mm. The time (T) between peaks or troughs is estimated using a correlation-based algorithm, from which the propagation speed c is estimated (c = 2/T). A parametric map of shear wave speed is generated for the entire ROI (center map) with a color scale depicting soft (blue) to stiff (red) tissues, opposite to what is typically used in compression-based schemes. A quality factor map (far right) based on signal-to-noise ratio and correlation coefficient is included. Accuracy is determined by sampling between shear waves. If the peaks are well-defined, as in this case, without broadening, the time domain correlation gives accurate estimates*

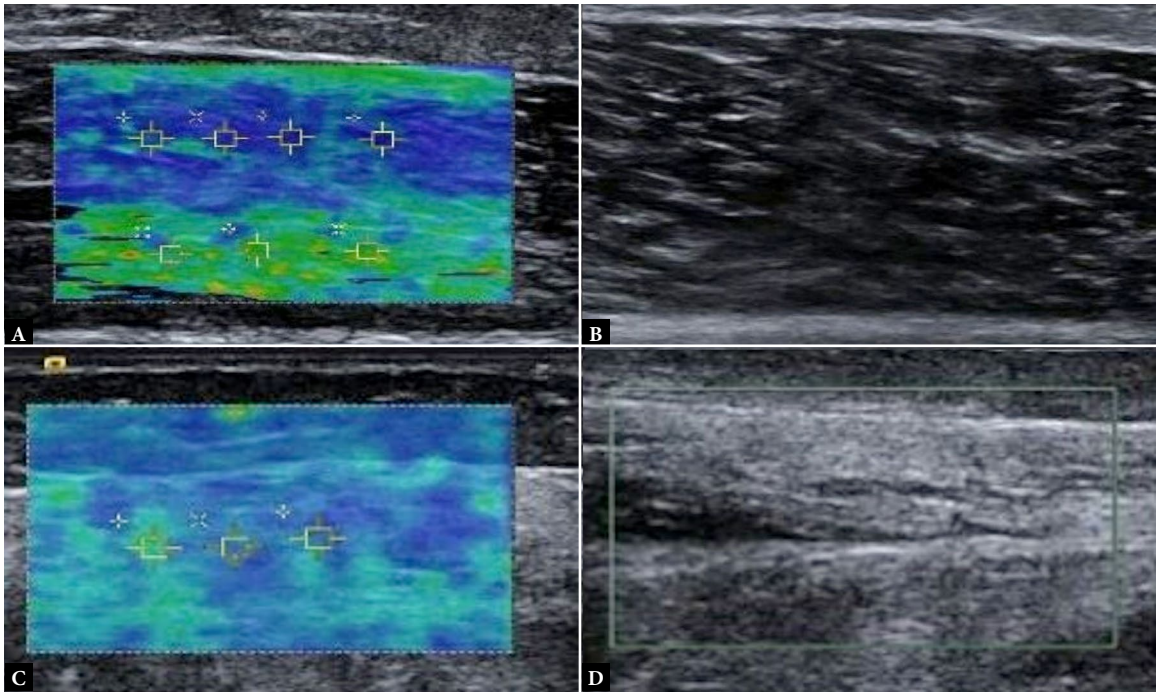

Fig. 19. *Shear wave elastography (SWE) in a normal volunteer (***A**, **B***) versus a patient with and underlying chronic myopathic disorder (***C**, **D***). Images obtained from the medial gastrocnemius muscle in long axis and corresponding SWE parametric image. Additional point quantifications listed from randomly placed samples within each ROI. Images from an asymptomatic 33-year-old female show shear wave elastogram (A) and normal muscle morphology on grayscale (B) with shear wave speeds > 2 m/s up to 3 m/s (not shown). Shear wave elastogram in a 39-year-old female patient with a myopathic disorder (C) and corresponding grayscale ultrasound (D). The shear wave speeds are less than 2 m/s (not shown). The corresponding grayscale image (D) depicts a diffusely echogenic muscle with loss of normal fascicular morphology, compatible with atrophy*

measure or parametric map of soft tissue stiffness. In this respect, SWE has been useful to produce more global and quantitative soft tissue assessment. SWE has been used to study tendon, ligament, joint and muscle abnormalities with encouraging preliminary results, although large controlled series are still lacking[99–105] (Fig. 19).

A limitation of SWE is the lack of uniformity across different scanners, or when using different transducers within the same scanner. The parametric images are of low spatial resolution due to the method used to track wave propagation. Two additional problems also arise in shear wave imaging, which have not as yet been addressed by vendors. Musculoskeletal soft tissues are inherently anisotropic, so that measurements of shear elastic or Young's modulus are directionally dependent[97,100,106]. Two-dimensional tracking techniques, using matrix arrays, may ultimately deal with this issue by displaying the angle-dependent two-dimensional propagation patterns following a cylindrically symmetric push pulse. Secondly, the shear wave speed is frequency-dependent at the higher end of the frequency spectrum due to viscoelastic effects[100,106]. This is not generally taken into consideration in any clinically available system, although it is an area of ongoing research.

Harmonic imaging

Much of ultrasound is based on the assumption of a fixed speed of sound in soft tissue. An approximate plane wave of a given frequency reflects off a surface and is reflected back to the transducer, a coherent process, or the wave can undergo scattering by point-like scatterers, which is an incoherent process. This is complicated by attenuation, which exponentially diminishes the pressure amplitude with a decay coefficient proportional to frequency. To a first approximation, many of these processes can be understood as being linear: an example being scattering of a plane wave from a point scatterer. The propagation of sound in biological soft tissues, however, is inherently non-linear, particularly at high enough pressure amplitudes. During the compressional phase, the speed of sound increases slightly, whereas during relaxation the speed of sound will decrease. The extent to which this non-linearity should be taken into account is determined by the non-linearity factor, B/A[107,108].

Tissue harmonics

When B/A is sufficiently large, higher order harmonics will be generated; the wave is no longer represented as a simple plane wave but rather as a summation of waves consisting of higher order terms, each propagating at some multiple of the original (or fundamental) frequency. These higher order terms can be scattered back to the transducer (Fig. 20). Detection of these lower amplitude harmonics can have a number of distinct advantages, such as improved signal-to-noise ratio, contrast, and axial and lateral resolution[109]. Harmonic imaging generally refers to second harmonic detection (propagates at twice the fundamental frequency) and imaging. A broadband transducer operating at a lower center frequency (i.e., 6 MHz) can transmit into the soft tissue, being less susceptible to attenuation. The second harmonic frequency (12 MHz) can be detected to produce a higher axial resolution image (Fig. 21), which is less attenuated at the higher frequency due to the shortened propagation distance. Tissue harmonic imaging (THI) is particularly well-suited to deeper structures, such as the supraspinatus tendon, muscle or interdigital web spaces, where subcutaneous fat can be problematic. In scanning very superficial structures, THI is less of an advantage[110].

Contrast harmonics

Second-harmonic imaging has become the method of choice when used in conjunction with contrast agents[111]. Bubbles oscillate at a resonant frequency corresponding to the appropriate insonating frequency (fundamental), to generate higher order harmonics in the backscattered wave. The corresponding waves are of significantly higher amplitude (orders of magnitude) in comparison to backscattered waves that derive from scatterers within the soft tissue. In this manner, areas of enhancement are selectively imaged. There are a variety of methods used to detect these harmonic waves, including

Fig. 20. *Tissue non-linearity. A simulated sinusoidal wave from the transducer is continuously distorted at increasing depths due to variation in the speed of sound in soft tissue. In the compressional phase, the propagation speed increases, whereas it decreases during decompression. As the wave propagates, it undergoes progressive distortion from a sinusoidal wave in the near field to a sawtooth pattern at increasing depth. This distorted wave can be represented as a Fourier series containing higher harmonic contributions, the dominant being the second harmonic (twice the transmit or fundamental frequency). The backscattered second harmonic is detected, allowing higher spatial resolution with less attenuation*

frequency selection, pulse inversion or amplitude modulation[111]. The resulting image displays the distribution of microbubbles over time on a capillary level, allowing quantitative estimates of soft tissue perfusion and blood volume (Fig. 14, Video 1).

Interventional ultrasound

With the appearance of real-time grayscale imaging in the late 1970s/early 1980s, and noting the conspicuity of metallic needles relative to adjacent soft tissue anatomy, a large variety of procedures have been shown to be readily performed under ultrasound guidance[17,112]. Since fluid is of high contrast on ultrasound, the earliest musculoskeletal applications (1980s/1990s) included joint and cyst aspirations[113–115]. Subsequently, ultrasound guidance was shown to be useful in performing a large variety of musculoskeletal interventions, including bursal, tendon sheath and joint injections, and in the treatment of calcific tendinosis[14,116]. In recent years, ultrasound has been also used extensively in perineural blocks and therapeutic injections as well as for localization for ablative therapy, such as alcohol, RF and cryoablations[117,118] (Fig. 2, Fig. 3).

The majority of technical developments during this period relate to the compactness of the ultrasound scanners and transducers, which have become more portable along with the availability of smaller footprint transducers (e.g., hockey stick) and higher operating frequencies[15–17]. Efforts to increase needle conspicuity, such as beam steering and echo tip needles, have been developed to improve confidence during needle positioning.

Since many procedures are performed in patients who already have pre-existing imaging in the form of computed tomography (CT) or

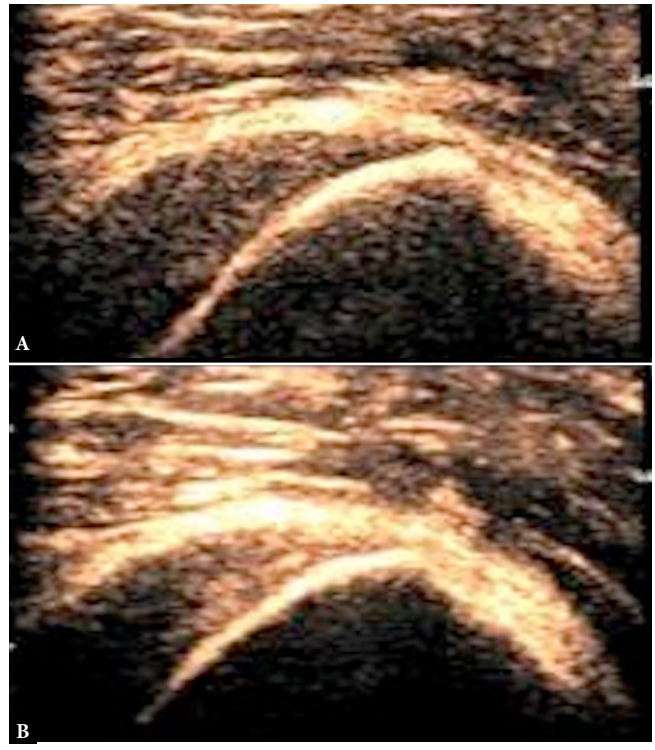

Fig. 21. *Tissue harmonic imaging (THI). Images of the rotator cuff with (***A***) and without (***B***) THI, using an 18L6 MHz linear transducer (Siemens Sequoia, Siemens Medical Systems). No spatial compounding is applied for purposes of comparison. An improvement in soft tissue detail is evident with tissue harmonics applied. The axial and contrast resolution are improved at the higher harmonic components. Tissue boundaries are more distinct, and the speckle spot size appears smaller*

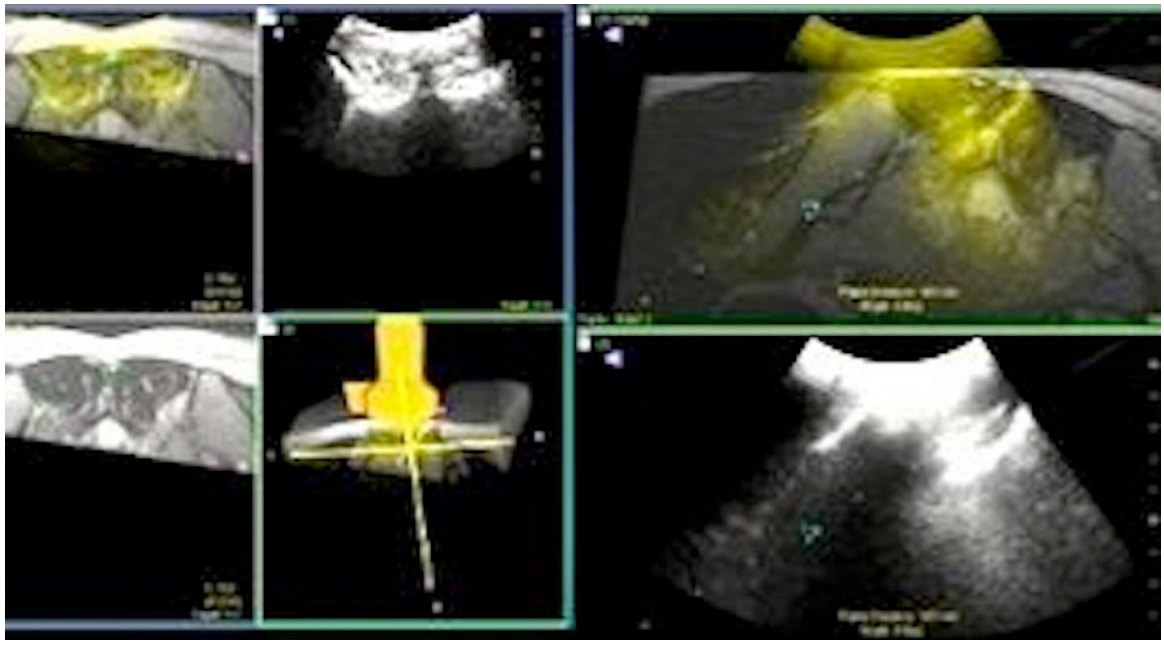

Fig. 22. *Planning for sacroiliac (SI) joint injection using an axial MR image of the pelvis for registration (left). An electromagnetic field generator is used with sensors placed on the transducer, sometimes on the patient and on the needle to help localize these in space. Common fiduciary markers are used to achieve registration. Usually, a minimum of three points are chosen. The transducer position, corresponding MR and US images are displayed as well as the juxtaposition of MR and ultrasound images. In the right images, a needle trajectory is simulated and superimposed on the ultrasound and composite ultrasound/MR images. The needle trajectory is seen to enter the joint proper on the juxtaposed image*

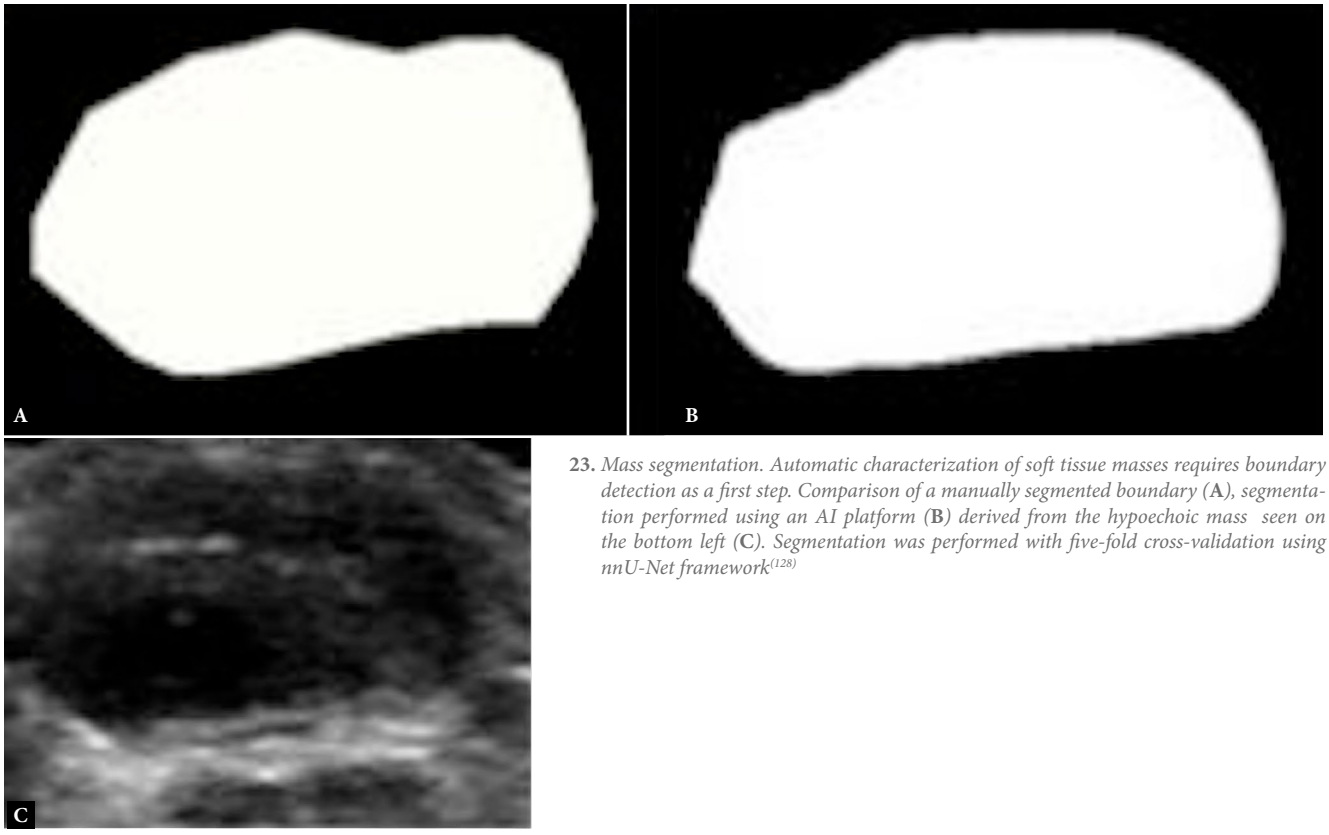

23. *Mass segmentation. Automatic characterization of soft tissue masses requires boundary detection as a first step. Comparison of a manually segmented boundary (***A***), segmentation performed using an AI platform (***B***) derived from the hypoechoic mass seen on the bottom left (***C***). Segmentation was performed with five-fold cross-validation using nnU-Net framework*[128]

magnetic resonance imaging (MRI), image co-registration capabilities have been added to more advanced ultrasound systems over the last 10–15 years[119] (Fig. 22). These largely entail the use of an electromagnetic field generator to localize the transducer location and orientation in space, identifying common fiduciary markers between both sets of imaging data (ultrasound/CT or ultrasound/MRI) and using the least squares techniques to calculate the appropriate mathematical transformation to superimpose both imaging data sets. Likewise, a transmitter can be placed on a needle to localize it in the image space during positioning. One can then effectively scan using either ultrasound or CT/MRI in a real-time setting to identify a target area for injection, aspiration or biopsy[120–121]. While these systems have proven to be useful in a variety of musculoskeletal procedures, where the target is not readily visualized on a baseline ultrasound, they continue to be somewhat cumbersome and potentially expensive for routine applications.

Artificial intelligence (AI)

Applications of AI to the musculoskeletal system have received a great deal of attention in the last decade[122]. These techniques have been shown to be particularly adept at classifying and identifying soft tissue pathology, as well as performing image segmentation (Fig. 23). Convolutional neural networks (CNN) and deep learning (DL) techniques in particular are proficient at image analysis and will likely be implemented as aids to radiologic interpretation and improvements to workflows in the near future[123,124].

With respect to image analysis, most applications involve a supervised learning approach, whereby a series of input images are used to train the CNN, which entails using a series of filters applied to the data, determining whether there are any dominant features present in the convolved data set, and pooling those features to be compared with a set of truth data. Examples would include detection of tissue boundaries or lesion classification. The operations may be computationally intensive, but are well-suited to the capabilities of the current generation of high-end ultrasound scanners. Based on the author's experience, these have only been used for relatively simple applications to date, although the current literature has demonstrated promising applications for MSKUS in inflammatory arthritis, segmentation of muscular anatomy, and lesion characterization[125–127].

Summary

MSKUS has developed rapidly over the last 40 years, paralleling advances in ultrasound technology, software, and hardware in accordance with Moore's law. The appearance of a large variety of transducer capabilities and rapid image processing, along with the ability to assess vascularity and tissue properties, has already expanded and continues to expand the role of MSKUS. It should also be recognized that these developments have in large part been possible due to a number of individuals who had the insight to see the potential applications of this developing technology to a host of relevant clinical musculoskeletal problems.

Exquisite high-resolution images of both deep and small superficial musculoskeletal anatomy, assessment of vascularity on a capillary level and tissue mechanical properties can be obtained. Ultrasound has also been recognized as the method of choice to perform a large

variety of interventional procedures. Time-dependent 3-D imaging along with automatic image analysis depicting abnormal tissue morphology and function, as well as greater sophistication in performing interventions, may be natural outgrowths of these developments.

Conflict of interest

The author does not report any financial or personal connections with other persons or organizations which might negatively affect the contents of this publication and/or claim authorship rights to this publication.

References

1. Holmes JH, Howry DH, Posakony GJ, Cushman CR: The ultrasonic visualization of soft tissue structures in the human body. Trans Am Clin Climatol Assoc 1954; 66: 208–225.
2. McNally EG: The development and clinical applications of musculoskeletal ultrasound. Skeletal Radiol 2011; 40: 1223–1231. https://doi.org/10.1007/s00256-011-1220-5.
3. van Holsbeeck M, Soliman S, Van Kerkhove F, Craig J: Advanced musculoskeletal ultrasound techniques: what are the applications. AJR Am J Roentgenol 2021; 216: 436–445. https://doi.org/10.2214/ajr.20.22840.
4. Sheng Z, Smith J, Kim K: Current status and advancement of ultrasound imaging technologies in musculoskeletal studies. Curr Phys Med Rehabil Rep 2022; 10: 45–51. https://doi.org/10.1007/s40141-021-00337-0.
5. Lin CY, Ooi CC, Chan E, Chew KT: Emerging technological advances in musculoskeletal ultrasound. PM R 2018; 10: 112–119. https://doi.org/10.1016/j.pmrj.2017.08.444.
6. Lento PH, Primac S: Advances and utility of diagnostic ultrasound in musculoskeletal medicine. Curr Rev Musculoskelet Med 2008; 1: 24–31. https://doi.org/10.1007/s12178-007-9002-3.
7. Sharpe RE, Nazarian LN, Parker L, Rao VM, Levin DC: Dramatically increased musculoskeletal ultrasound utilization from 2000 to 2009, especially by podiatrists in private offices. J Am Coll Radiol 2012; 9: 141–146. https://doi.org/10.1016/j.jacr.2011.09.008.
8. Bureau NJ, Ziegler D: Economics of musculoskeletal ultrasound. Curr Radiol Rep 2016; 4: 44, 1–7. https://doi.org/10.1007/s40134-016-0169-5.
9. Klauser AS, Tagliafico A, Allen GM, Boutry N, Campbell R, Court-Payen M *et al.*: Clinical indications for musculoskeletal ultrasound: a Delphi-based consensus paper of the European society of musculoskeletal radiology. Eur Radiol 2012; 22: 1140–1148. https://doi.org/10.1007/s00330-011-2356-3.
10. Kane D, Balint PV, Sturrock R, Grassi W: Musculoskeletal ultrasound – a state of the art review in rheumatology. Part 1: Current controversies and issues in the development of musculoskeletal ultrasound in rheumatology. Rheumatology 2004; 43: 823–882. https://doi.org/10.1093/rheumatology/keh214.
11. Spencer JK, Adler RS: Utility of portable ultrasound in a community in Ghana. J Ultrasound Med 2008; 27: 1735–1743. https://doi.org/10.7863/jum.2008.27.12.1735.
12. Wynter Bee W, Thing J: Ultrasound-guided injections in primary care: evidence, costs, and suggestions for change. Brit J General Pract 2017; 67: 378–379. https://doi.org/10.3399/bjgp17x692117.
13. Zardi EM, Franceschetti E, Giorgi C, Palumbo A, Franceschi F: Accuracy and performance of a new handheld ultrasound machine with wireless system. Sci Rep 2019; 9: 14599. https://doi.org/10.1038/s41598-019-51160-6.
14. Sofka CM, Collins AJ, Adler RS: Utilization of ultrasound guidance in interventional musculoskeletal procedures: a review from a single institution. J Ultrasound Med 2001; 20: 21–26. https://doi.org/10.7863/jum.2001.20.1.21.
15. Shung KKJ: Diagnostic ultrasound: past, present, and future. J Med Biol Eng 2011; 31: 371–374. http://dx.doi.org/10.5405/jmbe.871.
16. Dietrich CF, Bolondi L, Duck F, Evans DH, Ewertsen C, Fraser AG, Gilja OH *et al.*: History of ultrasound in medicine from its birth to date (2022), on occasion of the 50 Years Anniversary of EFSUMB. A publication of the European Federation of Societies for Ultrasound In Medicine and Biology (EFSUMB), designed to record the historical development of medical ultrasound. Med Ultrason 2022; 24: 434–450. https://doi.org/10.11152/mu-3757.
17. Nielsen MB, Søgaard SB, Andersen SB, Skjoldbye B, Hansen KL, Rafaelsen S *et al.*: Highlights of the development in ultrasound during the last 70 years: A historical review, Acta Radiol 2021; 62: 1499–1514. https://doi.org/10.1177/02841851211050859.
18. Szabo TL: Turning points in diagnostic ultrasound. In: Halliwell M, Wells PNT (eds): Acoustical Imaging, vol. 25, Springer New York, NY 2002: 1–6. https://doi.org/10.1007/b117160.
19. Santo B, Wollard K: The world of silicon: it's dog eat dog. IEEE Spectrum 1978; 25: 30–39.
20. Fornage BD: Achilles tendon ultrasound examination. Radiology 1986; 159: 759–764. https://doi.org/10.1148/radiology.159.3.3517959.
21. Graf R: The diagnosis of congenital hip-joint dislocation by the ultrasonic Combound treatment. Arch Orthop Trauma Surg 1980; 97: 117–133. https://doi.org/10.1007/bf00450934.
22. Middleton WD, Edelstein G, Reinus WR, Melson GL, Murphy WA.: Ultrasound of the rotator cuff: technique and normal appearance. J Ultra Med 1984; 3: 549–551. https://doi.org/10.7863/jum.1984.3.12.549.
23. Shi J, Mandell JC, Burke CJ, Adler RS, Beltran LS: Review of interventional musculoskeletal US techniques. Radiographics 2020; 40: 1684–1685. https://doi.org/10.1148/rg.2020200036.
24. Carson PL, Wenzel WW, Avery P, Hendee WR: Ultrasound imaging as an aid to cancer therapy II. Int J Radiat Oncol Biol Phys 1976; 1: 335–343. https://doi.org/10.1016/0360-3016(76)90064-x.
25. McDonald DG, Leopold GR: Ultrasound B-scanning in the differentiation of Baker's cyst and thrombophlebitis. Br J Radiol 1972; 45: 729–732. https://doi.org/10.1259/0007-1285-45-538-729.
26. Hamilton JV, Flinn Jr G, Haynie CC, Cefalo RC: Diagnosis of rectus sheath hematoma by B mode ultrasound: a case report. Obstet Gynecol 1976; 125: 562–565. https://doi.org/10.1016/0002-9378(76)90379-3.
27. Zweymueller K, Kratochwil A: Ultrasound diagnosis of bone and soft tissue tumors. Wien Klin Wochenschr 1975; 87: 397–398.
28. Kramer FL, Kurtz AB, Rubin C, Goldberg BB: Ultrasound appearance of myositis ossificans. Skelet Radiol 1979; 4: 19–20. https://doi.org/10.1007/bf00350588.
29. Wicks JD, Silver TM, Bree RL: Gray scale features of hematomas: an ultrasonic spectrum. Am J Roentgenol 1978; 131: 977–980. https://doi.org/10.2214/ajr.131.6.977.
30. Kumari S, Fulco JD, Karayalcin G, Lipton R: Gray scale ultrasound: evaluation of iliopsoas hematomas in hemophiliacs. Am J Roentgenol 1979; 133: 103–106. https://doi.org/10.2214/ajr.133.1.103.
31. Cooperberg PL, Tsang I, Truelove L, Knickerbocker WJ: Gray scale ultrasound in the evaluation of rheumatoid arthritis of the knee. Radiology 1978; 126: 759–763. https://doi.org/10.1148/126.3.759.
32. Gompels BM, Darlington LG: Septic arthritis in rheumatoid disease causing bilateral shoulder dislocation: diagnosis and treatment assisted by grey scale ultrasonography. Ann Rheum Dis 1981, 40, 609–611. https://doi.org/10.1136/ard.40.6.609.
33. Heckmatt JZ, Leeman S, Dubowitz V: Ultrasound imaging in the diagnosis of muscle disease. J Pediatr 1982; 101: 656–660. https://doi.org/10.1016/s0022-3476(82)80286-2.
34. Aisen AM, McCune WJ, MacGuire A, Carson PL, Silver TM, Jafri SZ *et al.*: Sonographic evaluation of the cartilage of the knee. Radiology 1984; 153: 781–784. https://doi.org/10.1148/radiology.153.3.6387794.
35. László A, Gellén J: Ultrasonic B-scan in progressive muscular dystrophy in children. Orv Hetil 1982; 123: 1671–1673. In Hungarian.
36. Maner MB, Marsh MJ: Ultrasonic findings in a ruptured Achilles tendon. Med Ultrasound 1981; 5: 81–82.
37. Mayer R, Wilhelm K, Pfeifer KJ: Ultrasound examination of subcutaneous Achilles tendon rupture. Digit Bilddiagn 1984; 4: 185–189. In German.
38. Fornage BD, Touche DH, Segal P, Rifkin MD: Ultrasonography in the evaluation of muscular trauma. J Ultrasound Med 1983; 2: 549–554. https://doi.org/10.7863/jum.1983.2.12.549.
39. Middleton WD, Reinus WR, Totty WG, Melson CL, Murphy WA: Ultrasonographic evaluation of the rotator cuff and biceps tendon. J Bone Joint Surg Am 1986; 68: 440–450.
40. Fornage BD, Rifkin MD: Ultrasound examination of tendons. Radiol Clin North Am 1988; 26: 87–107.

41. Fornage BD, Rifkin MD: Ultrasound examination of the hand and foot. Radiol Clin North Am 1988; 26: 109–129.
42. Graf R: New possibilities for the diagnosis of congenital hip joint dislocation by ultrasonography. J Pediatr Orthop 1983; 3: 354–359. https://doi.org/10.1097/01241398-198307000-00015.
43. Marchal GJ, Van Holsbeeck MT, Raes M, Favril AA, Verbeken EE, Casteels-Vandaele M *et al.*: Transient synovitis of the hip in children: role of US. Radiology 1987; 162: 825–828. https://doi.org/10.1148/radiology.162.3.3544039.
44. Fornage BD: Periferal nerves of the extremities: imaging with US. Radiology 1988; 167: 176–182. https://doi.org/10.1148/radiology.167.1.3279453.
45. De Flaviis L, Scaglione P, Nessi R, Ventura R, Calori G: Ultrasonography of the hand in rheumatoid arthritis. Acta Radiol 1988; 29: 457–460.
46. van Holsbeeck M, van Holsbeeck K, Gevers KG, Marchal G, van Steen A, Favril A *et al.*: Staging and follow-up of rheumatoid arthritis of the knee. J Ultrasound Med 1988; 7: 561–566. https://doi.org/10.7863/jum.1988.7.10.561.
47. Cochran S, Bernassau A, Demore C., Cumming D, Desmulliez M., Sweet J: Future integration of silicon electronics with miniature piezoelectric ultrasonic transducers and arrays. 2010 IEEE International Ultrasonics Symposium (IUS), 2010: 1108–1116. https://orcid.org/0000-0001-7324-7790.
48. Wildes DG, Chiao RY, Daft CMW, Rigby KW, Smith LS, Thomenius KE:. Elevation performance of 1.25D and 1.5D tansducer arrays. IEEE Trans Ultrason Ferroelec Freq Control 1997; 44: 1027–1037.
49. Beaver WL, Maginness MG, Meindl JD: Ultrasonic imaging using two-dimensional transducer arrays. Proc. SPIE 0072, Cardiovascular Imaging and Image Processing: Theory and Practice 1976; 17–23. https://doi.org/10.1117/12.954636.
50. Fredfeldt KE, Holm HH, Pedersen JF: Three-dimensional ultrasonic scanning. Acta Radiol Diagn (Stockh) 1984; 25: 237–241. https://doi.org/10.1177/028418518402500313.
51. Snyder JE, Kisslo J, von Ramm O: Real-time orthogonal mode scanning of the heart. I. System design. J Am Coll Cardiol 1986; 7: 1279–1285. https://doi.org/10.1016/s0735-1097(86)80147-4.
52. Sohn C, Grotepss J, Menge KH, Ameling W: Clinical-application of 3-dimensional ultrasound display. Dtsch Med Wochenschr 1989; 114: 534–537. In German. https://doi.org/10.1055/s-2008-1066630.
53. Rubin JM, Bude RO, Carson PL, Bree RL, Adler RS**:** Power doppler US: a potentially useful alternative to mean frequency – based color doppler US. Radiology 1994; 290: 853–856. https://doi.org/10.1148/radiology.190.3.8115639.
54. Newman JS, Adler RS, Bude RO, Rubin JM: Detection of soft tissue hyperemia; value of power doppler sonography. Am J Roentgenol 1994; 163: 385–389. https://doi.org/10.2214/ajr.163.2.8037037.
55. Newman JS, Laing TJ, McCarthy CJ, Adler RS: Power doppler sonography in synovitis: assessment of therapeutic response – preliminary observations. Radiology 1996; 198: 582–584. https://doi.org/10.1148/radiology.198.2.8596870.
56. Breidahl WH, Newman JS, Taljanovic MS, Adler RS: Power doppler assessment of musculoskeletal fluid collections. Am J Roentgenol 1996; 166: 1443–1446. https://doi.org/10.2214/ajr.166.6.8633460.
57. Breidahl WH, Stafford-Johnson DB, Newman JS, Adler RS**:** Power doppler sonography in tenosynovitis: significance of the peritendinous hypoechoic rim. J Ultrasound Med. 1998; 17: 103–107. https://doi.org/10.7863/jum.1998.17.2.103.
58. Wakefield RJ, Brown AK, O'Connor PJ, Emery P: Power doppler sonography: improving disease activity assessment in inflammatory musculoskeletal disease. Arthritis Rheum 2003; 48: 285–288. https://doi.org/10.1002/art.10818.
59. Rubin JM**,** Adler RS**,** Fowlkes JB, Spratt S, Pallister JE, Chen JF *et al.*: Fractional moving blood volume: estimation using power doppler US. Radiology 1995; 197: 183–190. https://doi.org/10.1148/radiology.197.1.7568820.
60. Demené C, Deffieux T, Pernot M, Osmanski B-F, Biran V, Gennisson J-L *et al.*: Spatiotemporal clutter filtering of ultrafast ultrasound data highly increases doppler and fUltrasound sensitivity. IEEE Trans Med Imaging 2015; 34: 1–17. https://doi.org/10.1109/tmi.2015.2428634.
61. Park AY, Seo BK, Woo OH, Jung KS, Cho KR, Park EK *et al.*: The utility of ultrasound superb microvascular imaging for evaluation of breast tumour vascularity: comparison with colour and power Doppler imaging regarding diagnostic performance. Clin Radiol 2018; 73: 304–311. https://doi.org/10.1016/j.crad.2017.10.006.
62. Lim AKP, Satchithananda K., Dick EA, Abraham S, Cosgrove DO: Microflow imaging: New Doppler technology to detect low-grade inflammation in patients with arthritis. Eur Radiol 2018; 128: 1046–1053. https://doi.org/10.1007/s00330-017-5016-4.
63. Gramiak R, Shah PM, Kramer DH: Ultrasound cardiography: Contrast studies in anatomy and function. Radiology 1969; 92: 939–948. https://doi.org/10.1148/92.5.939.
64. Frinking P, Segers T, Luan Y, Tranquart F: Three decades of ultrasound contrast agents: a review of the past, present and future improvements. Ultrasound Med Biol 2020; 46: 892–908. https://doi.org/10.1016/j.ultrasmedbio.2019.12.008.
65. Averkiou MA, Bruce MF, Powers JE, Sheeran PS, Burns PN: Imaging methods for ultrasound contrast agents. Ultrasound Med Biol 2020; 46: 498–517. https://doi.org/10.1016/j.ultrasmedbio.2019.11.004.
66. Klauser A, Frauscher F, Schirmer M, Halpern E, Pallwein L, Herold M *et al.*: The value of contrast-enhanced color Doppler ultrasound in the detection of vascularization of finger joints in patients with rheumatoid arthritis. Arthritis Rheum 2002; 46: 647–653. https://doi.org/10.1002/art.10136.
67. Klauser A, Demharter J, De Marchi A, Sureda D, Barile A, Masciocchi C *et al.* Contrast enhanced gray-scale sonography in assessment of joint vascularity in rheumatoid arthritis: results from the IACUS study group. Eur Radiol 2005; 15: 2404–2410. https://doi.org/10.1007/s00330-005-2884-9.
68. Krix, M, Weber MA, Krakowski-Roosen H, Huttner HB, Delorme S, Kauczor H-U *et al.*: Assessment of skeletal muscle perfusion using contrast-enhanced ultrasonography. J Ultrasound Med 2005; 24: 431–441. https://doi.org/10.7863/jum.2005.24.4.431.
69. Weber MA, Krix M, Delorme S: Quantitative evaluation of muscle perfusion with CEUS and with MR. Eur Radiol 2007; 17: 2663–2674. https://doi.org/10.1007/s00330-007-0641-y.
70. Rudzki JR, Adler RS, Warren RF, Kadrmas WR, Verma N, Pearle A *et al.*: Contrast enhanced ultrasound characterization of the vascularity of the rotator cuff tendon: age and activity related changes in the intact asymptomatic rotator cuff. J Shoulder Elbow Surg; 17: 96S–100S. https://doi.org/10.1016/j.jse.2007.07.004.
71. Adler RS, Fealy S, Rudzki J, Kadrmas W, Verma N, Pearle A *et al.*: Contrast enhanced ultrasound imaging of the rotator cuff in asymptomatic volunteers: depiction of intra and peritendinous vascularity. Radiology 2008; 248: 954–961. https://doi.org/10.1148/radiol.2483071400.
72. Chaudhury S, de La Lama M, Adler RS, Gulotta LV, Skonieczki B, Chang A *et al.*: Platelet-rich plasma for the treatment of lateral epicondylitis: sonographic assessment of tendon morphology and vascularity (pilot study). Skeletal Radiol 2013; 42: 91–97. https://doi.org/10.1007/s00256-012-1518-y.
73. Burckhardt CB: Speckle in ultrasound B-mode scans. IEEE Trans Son Ultrason 1978; 25: 1–6.
74. Wagner RF, Insana MF, Brown DG: Statistical properties of radio-frequency and envelope-detected signals with applications to medical ultrasound. J Opt Soc Am 1987; 4: 910–922. https://doi.org/10.1364/josaa.4.000910.
75. Wagner RF, Insana MF, Smith SW: Fundamental correlation lengths of coherent speckle in medical ultrasound images. IEEE Trans Ultrason Ferroelectr Freq Control 1988; 35: 34–44. https://doi.org/10.1109/58.4145.
76. Trahey G., Smith S., von Ramm O: Speckle pattem correlation with lateral aperture translation: experimental results and implications for spatial compounding. IEEE Trans Ultrason Ferroelectr Freq Control 1986; 33: 257–264. https://doi.org/10.1109/t-uffc.1986.26827.
77. Hankar PM: Speckle reduction in ultrasound b-scans using weighted averaging in spatial compounding. IEEE Trans Ultrason Ferroelectr Freq Control 1986; 33: 754–758. https://doi.org/10.1109/t-uffc.1986.26892.
78. Berson M, Roncin A, Pourcelot L: Compound scanning with an electrically steered beam. Ultrasonic Imaging 1981; 3: 303–308.
79. Jespersen SK, Wilhjelm JE, Sillesen H: Multi-angle compound imaging. Ultrasonic Imaging 1998; 20: 81–102. https://doi.org/10.1177/016173469802000201.
80. Park J, Kang JB, Chang JH, Yoo Y: Speckle reduction techniques in medical ultrasound imaging. Biomed Eng Lett 2014; 4: 32–40. http://dx.doi.org/10.1007/s13534-014-0122-6.
81. Entrekin RR, Porter BA, Sillesen HH, Wong AD, Cooperberg PL, Fix CH: Real-time spatial compound imaging: application to breast, vascular, and musculoskeletal ultrasound. Semin Ultrasound CT MRI 2001; 22: 50–64. https://doi.org/10.1016/s0887-2171(01)90018-6.
82. Lin CD, Nazarian LN, O'Kane Pl, McShane JM, Parker L, Merritt CRB: Advantages of real-time compound sonography of the musculoskeletal system versus conventional sonography. AJR Am J Roentgenol 2002; 171: 1629–1631. https://doi.org/10.2214/ajr.179.6.1791629.
83. Chen EJ, Jenkins WK, O'Brien Jr WD: Performance of ultrasonic speckle tracking in various tissues. J Acoust Soc Am 1995; 98: 1273–1278. https://doi.org/10.1121/1.414453.
84. Barberie JE, Wong AD, Cooperberg PL, Carson BW: Extended field-of-view sonography in musculoskeletal disorders. AJR Am J Roentgenol 1998; 171: 751–757. https://doi.org/10.2214/ajr.171.3.9725310.
85. Lin EC, Middleton WD, Teefey SA: Extended field of view sonography in musculoskeletal imaging. J Ultrasound Med 1999; 18: 147–152. https://doi.org/10.7863/jum.1999.18.2.147.

86. Cooperberg PL, Barberie JJ, Wong T, Fix C: Extended field-of-view ultrasound. Semin Ultrasound CT MRI 2001; 22: 65–77. https://doi.org/10.1016/s0887-2171(01)90019-8.
87. Sarvazyan AP, Skovoroda AR, Emelianov SY, Fowlkes JB, Pipe JG, Adler RS *et al.*: Biophysical basis of elasticity imaging. In: Jones JP (ed): Acoustical Imaging, vol. 21. Plenum Press, New York 1995: 223–220.
88. Ophir J, Cespedes I, Ponnekanti H, Yazdi Y, Li X: Elastography: a quantitative method for imaging the elasticity of biological tissues. Ultrason Imaging 1991; 13: 111–134. https://doi.org/10.1177/016173469101300201.
89. Garra BS, Cespedes EI, Ophir J, Spratt SR, Zuurbier RA, Magnant CM *et al.*: Elastography of breast lesions: initial clinical results. Radiology 1997; 202: 79–86. https://doi.org/10.1148/radiology.202.1.8988195.
90. Shiina T: JSUM ultrasound elastography practice guidelines: basics and terminology. J Med Ultrasonics 2013; 40: 309–323. https://doi.org/10.1007/s10396-013-0490-z.
91. De Zordo T, Lill SR, Fink C, Feuchtner GM, Jaschke W, Bellmann-Weiler R *et al.*: Value of real-time sonoelastography in lateral epicondylitis: comparison of findings between patients and healthy volunteers. AJR Am J Roentgenol 2009; 193: 180–185. https://doi.org/10.2214/ajr.08.2020.
92. Klauser AS, Miyamoto H, Tamegger M, Faschingbauer R, Moriggl B, Klima G *et al.*: Achilles tendon assessed with sonoelastography: histologic agreement. Radiology 2013; 267: 837–842. https://doi.org/10.1148/radiol.13121936.
93. Yamamoto Y, Yamaguchi S, Sasho T, Fukawa T, Akatsu Y, Nagashima K *et al.*: Quantitative ultrasound elastography with an acoustic coupler for achilles tendon elasticity measurement repeatability and normative values. J Ultrasound Med 2016; 35:1 59–166. https://doi.org/10.7863/ultra.14.11042.
94. Nightingale KR, Palmeri ML, Nightingale RW, Trahey GE: On the feasibility of remote palpation using acoustic radiation force. J Acoust Soc Am 2001; 110: 625–634. https://doi.org/10.1121/1.1378344.
95. Nightingale K, Soo MS, Nightingale R, Trahey G: Elastography of breast lesions: initial clinical results. Radiology. Ultrason Med Biol 2002; 28: 227–235.
96. Lerner RM, Parker KJ, Holen J, Gramiak R, Waag RC: Sono-elasticity: medical elasticity images derived from ultrasound signals in mechanically vibrated targets. Acoust Imag 1988, 16: 317–327.
97. Gennisson JL, Catheline S, Chaffai S, Fink M: Transient elastography in anisotropic medium: application to the measurement of slow and fast shear wave speeds in muscles. J Acoust Soc Am 2003; 114: 536–541. https://doi.org/10.1121/1.1579008.
98. Taljanovic MS, Gimber LH, Becker GW, Latt LD, Klauser AS, Melville DM *et al.*: Shear-wave elastography: basic physics and musculoskeletal applications. Radiographics 2017; 37: 855–870. https://doi.org/10.1148/rg.2017160116.
99. Eby SF, Song P, Chen S, Chen Q, Greenleaf JF, An K-N: Validation of shear wave elastography in skeletal muscle. J Biomech 2013; 46: 2381–2387. https://doi.org/10.1016/j.jbiomech.2013.07.033.
100. Chen S, Fatemi, M, Greenleaf JF: Quantifying elasticity and viscosity from measurement of shear wave speed dispersion. J Acoust Soc Am 2004; 115: 2781–2785. https://doi.org/10.1121/1.1739480.
101. Carpenter EL, Lau HA, Kolodny EH, Adler RS: Skeletal muscle in healthy subjects versus those with GNE-related myopathy: evaluation with shea – wave US – a pilot study. Radiology 2015; 277: 546–554. https://doi.org/10.1148/radiol.2015142212.
102. Hou SW, Merkle AN, Babb JS, McCabe R, Gyftopoulos S, Adler RS: Shear wave ultrasound elastographic evaluation of the rotator cuff tendon. J Ultrasound Med 2017; 36: 95–106. https://doi.org/10.7863/ultra.15.07041.
103. Lin DJ, Burke CJ, Abiri B, Babb JS, Adler RS: Supraspinatus muscle shear wave elastography (SWE): detection of biomechanical differences with varying tendon quality prior to gray-scale morphologic changes. Skeletal Radiol 2020; 49: 731–738. https://doi.org/10.1007/s00256-019-03334-6.
104. Gimber LH, Daniel Latt L, Caruso C, Nuncio Zuniga AA, Krupinski EA, Klauser AS *et al.*: Ultrasound shear wave elastography of the anterior talofibular and calcaneofibular ligaments in healthy subjects. J Ultrason 2021; 21: e86–e94. https://doi.org/10.15557/jou.2021.0017.
105. Martinez JA, Taljanovic MS, Witte RS Nuncio Zuniga AA, Wertheim BC, Kwoh CK *et al.*: Shear wave elastography detects novel imaging biomarkers of aromatase inhibitor-induced joint pain: a pilot study. J Ultrason 2021; 21: 1–6. https://doi.org/10.15557/jou.2021.0001.
106. Gennisson JL, Deffieux T, Mace E, Montaldo G, Fink M, Tanter M *et al.*: Viscoelastic and anisotropic mechanical properties of in vivo muscle tissue assessed by supersonic shear imaging. Ultrasound Med Biol 2010; 36: 789–801. https://doi.org/10.1016/j.ultrasmedbio.2010.02.013.
107. Dunn F, Law WK, Frizzel LA: Nonlinear ultrasonic propagation in biological media. Br J Cancer Suppl 1982; 45: 55.
108. Law WK, Frizzell LA, Dunn F: Determination of the non-linearity parameter B/A of biological media. Ultrasound Med Biol 1985; 11: 307–318. https://doi.org/10.1016/0301-5629(85)90130-9.
109. Tranquart F, Grenier N, Eder V, Pourcelot L: Clinical use of ultrasound tissue harmonic imaging. Ultrasound Med Biol 1999; 25: 889–894. https://doi.org/10.1016/s0301-5629(99)00060-5.
110. Strobel K, Zanetti M, Nagy L, Hodler J: Suspected rotator cuff lesions: tissue harmonic imaging versus conventional US of the shoulder. Radiology 2004; 230: 243–249. https://doi.org/10.1148/radiol.2301021517.
111. Averkiou MA, Bruce MF, Powers JE, Sheeran PS, Burns PN: Imaging agents for ultrasound contrast agents. Ultrasound Med Biol 2020; 46: 498–517. https://doi.org/10.1016/j.ultrasmedbio.2019.11.004.
112. McGahan JP: The history of interventional ultrasound. J Ultrasound Med 2004; 23: 727–741. https://doi.org/10.7863/jum.2004.23.6.727.
113. Gompels BM, Darlington LG: Septic arthritis in rheumatoid disease causing bilateral shoulder dislocation: diagnosis and treatment assisted by grey scal. Ann Rheum Dis 1981; 40: 609–611. https://doi.org/10.1136/ard.40.6.609.
114. Breidahl WH, Adler RS: Ultrasound-guided injection of ganglia with corticosteroids. Skeletal Radiol 1996; 25: 635–638. https://doi.org/10.1007/s002560050150.
115. Farin PU, Rasanen H, Jaroma H, Harju A: Rotator cuff calcifications: treatment with ultrasound-guided technique percutaneous needle aspiration and lavage. Skeletal Radiol 1996; 25: 551–554. https://doi.org/10.1007/s002560050133.
116. Chiou H, Chou Y, Wu J, Hsu CC, Tiu CM, Chang CY *et al.*: Alternative and effective treatment of shoulder ganglion cyst: ultrasonographically guided aspiration. J Ultrasound Med 1999; 18: 531–535. https://doi.org/10.7863/jum.1999.18.8.531.
117. Adler RS**:** Percutaneous Ultrasound guided Interventions in the Musculoskeletal System. In: Rumack CM, Stephanie RW, Charboneau JW, Levine D (eds): Diagnostic Ultrasound, 4 Ed., Elsevier/Mosby, Philadelphia PA: 2011.
118. Shi J, Mandell JC, Burke CJ, Adler RS, Beltran LS: Review of interventional musculoskeletal US techniques. Radiographics 2020; 40: 1684–1685. https://doi.org/10.1148/rg.2020200036.
119. Ewertsen C, Săftoiu A, Gruionu LG, Karstrup S, Nielsen MB: Real-time image fusion involving diagnostic ultrasound. AJR Am J Roentgenol 2013; 200: W249-255. https://doi.org/10.2214/ajr.12.8904.
120. Klauser AS, De Zordo T, Feuchtner GM, Djedovic G, Weiler RB, Faschingbauer R *et al.*: Fusion of real-time US with CT images to guide sacroiliac joint injection in vitro and in vivo. Radiology 2010; 256: 547–553. https://doi.org/10.1148/radiol.10090968.
121. Burke CJ, Bencardino J, Adler R: The potential use of ultrasound-magnetic resonance imaging fusion applications in musculoskeletal intervention. J Ultrasound Med 2017; 36: 217–224. https://doi.org/10.7863/ultra.16.02024.
122. Fritz J, Kijowski R, Recht MP: Artificial intelligence in musculoskeletal imaging: a perspective on value propositions, clinical use, and obstacles. Skeletal Radiol 2022; 51: 239–243. https://doi.org/10.1007/s00256-021-03802-y.
123. Montero AB, Javaida U, Valdes G, Nguyen D, Desbordes P, Macq B *et al.*: Artificial intelligence and machine learning for medical imaging: a technology review. Phys Med 2021; 83: 242–256. https://doi.org/10.1016/j.ejmp.2021.04.016.
124. Fazala MI, Patela ME, Tyea J, Gupta Y: The past, present and future role of artificial intelligence in imaging. Eur J Radiol 2018; 105: 246–250. https://doi.org/10.1016/j.ejrad.2018.06.020.
125. Mielnik P, Fojcik M, Segen J, Kulbacki M: A novel method of synovitis stratification in ultrasound using machine learning algorithms: results from clinical validation of the MEDUSA project. Ultrasound Med Biol 2018; 44: 489–494. https://doi.org/10.1016/j.ultrasmedbio.2017.10.005.
126. Burlina P, Billings S, Joshi N, Albayda J: Automated diagnosis of myositis from muscle ultrasound: exploring the use of machine learning and deep learning methods. 2017; 12: e0184059. https://doi.org/10.1371/journal.pone.0184059.
127. Wang B, Perronne L, Burke C, Adler RS: Artificial intelligence for classification of soft-tissue masses seen on US. Radiol Artif Intell 2020; 3: e200125. https://doi.org/10.1148/ryai.2020200125.
128. Isensee F, Jaeger PF, Kohl SAA, Petersen J: nnU-Net: a self-configuring method for deep learning-based biomedical image segmentation. Nat Methods 2021; 18: 203–211. https://doi.org/10.1038/s41592-020-01008-z.